

Electronic Thesis and Dissertation Repository

---

4-18-2017 12:00 AM

## Study of the Dynamics and Cost Analysis of the Biogenerator

Tariq Abou Jarboua, *The University of Western Ontario*

Supervisor: Dr. Dimitre Karamanev, *The University of Western Ontario*

A thesis submitted in partial fulfillment of the requirements for the Master of Engineering Science degree in Chemical and Biochemical Engineering

© Tariq Abou Jarboua 2017

Follow this and additional works at: <https://ir.lib.uwo.ca/etd>

 Part of the [Chemical Engineering Commons](#)

---

### Recommended Citation

Abou Jarboua, Tariq, "Study of the Dynamics and Cost Analysis of the Biogenerator" (2017). *Electronic Thesis and Dissertation Repository*. 4491.

<https://ir.lib.uwo.ca/etd/4491>

This Dissertation/Thesis is brought to you for free and open access by Scholarship@Western. It has been accepted for inclusion in Electronic Thesis and Dissertation Repository by an authorized administrator of Scholarship@Western. For more information, please contact [wlsadmin@uwo.ca](mailto:wlsadmin@uwo.ca).

## Abstract

The BioGenerator is a promising energy storage solution that can be integrated with renewable power sources (i.e. wind and solar) to compensate the intermittent shortage of the renewable power sources and deliver a comprehensive power package. A trickling-bed bioreactor was considered to be used in the BioGenerator as an alternative to the initially studied "air-lift" type bioreactor. Trickling-bed bioreactor is well known for its low power consumption for oxygen transfer. Dynamic study was conducted on lab scale trickling-bed bioreactor to investigate the effect of the ferrous iron feed interruption on the iron biooxidation rate. The study showed that the iron biooxidation rate was temporary reduced by around 6% when the stoppage period was between 16 and 72 hours.

Also, a detailed cost analysis study was conducted to for 1 MW BioGenerator showing that its cost is very competitive option of energy storage, and can be used as an economical alternative to rechargeable batteries usually used with renewable power generation sources. The annualized capital cost of the BioGenerator is \$209,000/year, the capital cost per kW is \$3,000/kW, and the cost of electricity due to the BioGenerator is 6.2 cents per kWh.

## Keywords

BioGenerator, trickling-bed bioreactor, power storage of renewable energy, cost analysis of BioGenerator.

## Co-Authorship Statement

Tariq Abou Jarboua was the principal author. The supervisor Dr. Dimitre Karamanev made revisions and recommendations. Based on some results in this Thesis, two papers were prepared for submission to peer reviewed journals. The contribution of each author is shown below:

### **1. Study of the dynamics of ferrous iron biooxidation by *Leptospirillum ferriphilum* in a trickling bed bioreactor used for energy storage.**

Submitted to: *Biochemical Engineering Journal*.

Authors: *Tariq Abou Jarboua, Boris Nikolov and Dimitre Karamanev*

Experimental work and data analysis were performed by Tariq Abou Jarboua. The bioreactor design and start-up was performed by Boris Nikolov. Dr. Dimitre Karamanev provided consultation regarding experimental work and data analysis. The manuscript was written and revised by Tariq Abou Jarboua and reviewed by Dimitre Karamanev.

### **2. Economic analysis of a 1 megawatt microbial electrochemical cell, the BioGenerator.**

Submitted to: *Applied Energy Journal*

Authors: *Tariq Abou Jarboua, Dimitre Karamanev*

Scale-up design, material and equipment selection, and price estimation were performed by Tariq Abou Jarboua. Dr. Dimitre Karamanev provided price estimation of the electrochemical unit. The manuscript was written and revised by Tariq Abou Jarboua, and reviewed by Dimitre Karamanev.

## Acknowledgments

I would like to take the chance and express my sincere gratitude to my supervisor, Dr. Dimitre Karamanev for providing me the opportunity to work on this interesting project, and for his thorough guidance throughout the whole project.

Also, I would like to extend my appreciation to my parents, siblings and family for their great thrust and support, with very deep appreciation to my father for his continuous encouragement. Last but not least, I am grateful to my wife Eman, for her endless accommodation of proper climate for success.

# Table of Contents

Abstract .....	i
Co-Authorship Statement.....	ii
Acknowledgments.....	iii
Table of Contents .....	iv
List of Tables .....	vii
List of Figures .....	viii
Chapter 1 .....	1
1 Introduction .....	1
1.1 Renewable Energy .....	1
1.2 Energy Storage Technologies .....	6
1.3 References .....	14
Chapter 2.....	15
2 Literature Review.....	15
2.1 Fuel Cells Technology .....	15
2.2 Fuel Cell Types.....	20
2.2.1 Conventional Fuel Cells.....	20
2.2.2 Biological Fuel Cells.....	31
2.3 BioGenerator.....	34
2.4 BioGenerator Challenges .....	38
2.5 References.....	41
Chapter 3.....	43
3 Study of the Dynamics of Ferrous Iron Biooxidation by <i>Leptospirillum ferriphilum</i> in a Trickle Bed Bioreactor Used for Energy Storage .....	43
3.1 Introduction.....	43
3.2 Materials and Methods.....	45

3.2.1	Description of Experimental Setup.....	45
3.2.2	Microbial Culture and Liquid Medium.....	47
3.2.3	Biofilm Support Particles.....	48
3.2.4	Analytical Procedure.....	48
3.3	Results and Discussion .....	48
3.4	Conclusions.....	60
3.5	References.....	61
Chapter 4.....		62
4	Cost Analysis of a 1 Megawatt Bio-Electrochemical Technology, The BioGenerator	62
4.1	Nomenclature .....	62
	<i>Greek Letters</i> .....	64
	<i>Subscripts</i> .....	64
	<i>Abbreviations</i> .....	64
4.2	Introduction.....	65
4.2.1	BioGenerator.....	66
4.3	Purpose of This Study.....	68
4.4	BioGenerator Calculations.....	69
4.4.1	Overall Calculations.....	69
4.4.2	Bioreactor Calculations.....	70
4.4.3	Bioreactor Volume.....	71
4.4.4	Oxygen Requirement .....	71
4.4.5	Correction Factors for Oxygen Demand.....	72
4.4.6	Hydrogen Requirement.....	77
4.5	Sizing of Equipment .....	77
4.5.1	Sizing of the Bioreactor Tank and Other Civil Engineering and Construction Requirements.....	77

4.5.2	Sizing of Circulating Pumps .....	80
4.5.3	Sizing of Air Blowers .....	81
4.5.4	Sizing of Liquid and Air Pipelines.....	82
4.5.5	Electrical Supply.....	85
4.5.6	Mist Eliminator .....	85
4.5.7	Water Heater and Temperature Control.....	86
4.5.8	Electrochemical Cell Stacks .....	87
4.6	Cost Calculations .....	88
4.6.1	Civil and Construction Work.....	88
4.6.2	Circulating Pumps.....	91
4.6.3	Air Blowers.....	91
4.6.4	Air and Liquid Piping .....	91
4.6.5	Electrical and Control .....	93
4.6.6	Mist Eliminator .....	93
4.6.7	Water Heater and Temperature Controller .....	94
4.6.8	Electrochemical Cell Stack Units .....	94
4.6.9	Overall BioGenerator Cost Analysis .....	96
4.7	Discussion and Conclusion.....	99
4.8	References.....	100
Chapter 5	.....	103
5	Conclusions .....	103
Chapter 6	.....	105
6	Recommendations .....	105
Curriculum Vitae	.....	108

## List of Tables

Table 1. Classification of Fuel cells based on operating temperatures, used fuels and electrolytes .....	30
Table 2. Civil scope of work for the bioreactor tank and the plant room, estimated unit prices and the total cost of the work.....	89
Table 3. Pipeline quantities, their estimated unit prices and the total price.....	92
Table 4. Cost of all elements comprise the electrochemical stack unit. ....	95
Table 5. Summary of the individual and total capital cost of all BioGenerator components.	96



## List of Figures

Figure 1. Worldwide installed storage capacity for electrical energy (2010).....	8
Figure 2. Power to Gas (P2G) integrated with renewable energy .....	13
Figure 3. Schematic diagram of fuel cell system key components.....	16
Figure 4. Fuel Cell Electrochemistry .....	18
Figure 5. The configuration of fuel cell stack with multiple of single fuel cell components .	19
Figure 6. Basic structure and processes in PEM fuel cell, <a href="https://energy.gov/">https://energy.gov/</a> .....	21
Figure 7. The basic structure and processes in AFC, <a href="https://energy.gov/">https://energy.gov/</a> .....	23
Figure 8. The basic structure and processes in PAFC, <a href="https://energy.gov/">https://energy.gov/</a> . .....	25
Figure 9. The basic structure and processes in MCFC, <a href="https://energy.gov/">https://energy.gov/</a> . .....	27
Figure 10. The basic structure and processes of the SOFC, <a href="https://energy.gov/">https://energy.gov/</a> . .....	28
Figure 11. The basic structure and processes of the DMFC, <a href="http://www.intechopen.com">www.intechopen.com</a> . .....	29
Figure 12. Schematic representation of a typical MFC, <a href="https://biologicalfuelcell.com/">https://biologicalfuelcell.com/</a> .....	32
Figure 13. Schematic diagram of the BioGenerator .....	36
Figure 14. Typical time profile of wind power generation and smoothing to its average value. .....	44
Figure 15. Experimental setup of the trickling bed bioreactor. ....	46
Figure 16. Theoretical change of the substrate (ferrous ion) concentration in time during and after a feed flow interruption. ....	51
Figure 17. Experimental S-t curves for three hours feed flow interruption.....	53

Figure 18. The change of ferrous iron concentration in time for a 6 hours feed flow interruption.....	54
Figure 19. Effect of the 16 hours flow interruption on ferrous iron concentration. ....	55
Figure 20. Effect of the 24 hours flow interruption on ferrous iron concentration. ....	56
Figure 21. Effect of the 72 hours flow interruption on substrate concentration. ....	57
Figure 22. The relationship between the parameters $t_h$ and $t_s$ , as described in Fig. 15.....	58
Figure 23. The relationship between the parameters $S_h$ and $t_s$ , as described in Fig. 16.....	58
Figure 24. The effect of the parameter $t_s$ on the reduction of the ferrous iron biooxidation rate.....	59
Figure 25. Bioreactor concrete tank dimensional layout .....	79
Figure 26. Plant layout and the process flow diagram of the BioGenerator.....	85
Figure 27. Schematic view of the electrochemical stack used in the BioGenerator.....	88

## Chapter 1

# 1 Introduction

## 1.1 Renewable Energy

Transformation from the conventional power generation systems towards cheaper, renewable and environment-friendly resources has been motivating many researchers, governments and the private sector. There is no doubt that the current energy systems and technological advancements available in the world are not sufficient to stop the increase of the concentration of greenhouse gases that are emitted from those resources. We have to move quickly towards building new technologies and to bring the existing technologies together to rectify this issue and to get maximum benefit from the entire energy system including energy production, transformation, to energy transportation and distribution. A huge effort in this direction will have to be taken at both macro and micro levels.

Energy is critically important to the Canadian economy as Canada is among the largest energy producers and the highest per-capita energy consumers in the world because of our climate and resources.

As per Natural Resources Canada [1], electricity in Canada is generated from different and mixed sources. The electricity generated from natural and renewable resources such as water flow, nuclear, wind and solar is considered primary energy source while

electricity generated from consumed unrenovable resource such as fossil fuels (i.e. coal, natural gas and oil) is considered secondary energy.

Flowing water is the most important source in Canada, which generates 59.3 per cent of electricity supply. Canada is considered the second largest producer of hydroelectricity in the world after China, with over 378 terawatt hours in 2014. The installed hydropower capacity is more than 78 gigawatts. This capacity has been generated at favorable geography and hydrography locations, exist primarily in Quebec, but also in British Columbia, Ontario, Labrador and Manitoba.

The second most important source of electricity in Canada is fossil fuels. Coal has about 9.5 per cent of the generated electricity, while natural gas has the share of 8.5 per cent and 1.3 per cent goes to petroleum. Fossil fuel generation mostly exists in Alberta and Saskatchewan. Several power stations are located adjacent to large coal deposits. Fossil fuel generation is also significant in the Atlantic Provinces, Northwest Territories and Nunavut. As other provinces, Ontario was depending majorly on coal-fired generation; but not after April 2014 when the last coal-fired generating capacity was shut down.

The third most important source of electricity in Canada is nuclear power. It counts for about 16 per cent of generated electricity. Out of the Canada's nineteen operating nuclear power plants, eighteen are located in Ontario and one in New Brunswick. Quebec shut down their nuclear power plant in 2012.

From the non-hydro renewable sources, which contribute 5.2 per cent of the generated Canada's electricity, wind has become the major source and exceeded biomass (e.g.

wood waste, spent pulp liquor). However, solar power is still emerging but increasing rapidly to supply electricity.

As per Canadian Wind Energy Association (CanWEA) [2], Canada is growing fast in wind power generation, ending year 2015 with more than 11,000 MW of wind energy capacity, completed 36 wind power supply projects totaling 1,506 MW. At the same year Canada was the sixth largest market for new wind power supply globally, and presently has become the seventh largest wind generating capacity in the world.

The 36 wind projects of year 2015 value of \$3 billion in investment, were built and commissioned in Alberta, Saskatchewan, Ontario, Quebec and Nova Scotia. Out of those projects, 23 have significant ownership stakes from Aboriginal People, municipal corporations or local farmers.

Referring to the same study [2], the wind power generation is contributing approximately 5 per cent of Canada's electricity demand, which is the need of more than three million Canadian homes. This amount of power is supplied by 259 wind farms operating from coast to coast, including projects in two of the three northern territories.

It is expected that the Canadian wind industry's performance continues to strong and stable growth, and there are great opportunities to maximize the economic, industrial development, and environmental benefits associated with wind energy development.

A recent report from the Global Wind Energy Council (GWEC) [3], has forecasted a global increasing growth of wind power capacity around the world in the coming future.

The report also highlighted that the global wind industry has accomplished a record through year 2015, the total annual capacity installations were 63 GW and made up the total installed capacity of around 433 GW, presenting 17 % increase over the previous year. The total investment in new wind power development at year 2015 was almost \$ 110 billion, which makes the wind power the most popular choice for new power generation.

GWEC also reported that the overall total installed capacity in Asia is 175.8 GW putting Asia as the world's largest regional wind market. However, on national level, China is the leading with cumulative wind power installations of 145 GW which is greater than all European Union countries combined with capacity of 141.6 GW. Currently, 28 countries have a wind power capacity greater than 1 GW installed and eight countries have more than 10 GW installed.

The report further forecasted future wind capacity in 2050 would vary from a conservative 2,870 GW under the International Energy Agency's (IEA) New Policies Scenario, to its most ambitious 5,806 GW under the GWEC Advanced Scenario.

Under the GWEC Advanced Scenario, wind power is projected to provide at least 36 percent global electricity demand in 2050.

Electricity generated by wind is considered one of the fast-growing source of electricity worldwide. The wind turbine converts the kinetic energy produced by rotating mills due to the blow of the wind into an electrical energy. The wind turbines are erected in favorable weather patterns locations for higher expected production. Wind turbine can be

installed individually or with a group of turbines to form what it is called “wind farm” or “wind power plant”. Wind turbine and or wind farm can operate either locally (i.e. off grid) to serve specific user or community or can be connected to electricity on grid to serve with other power resources for greater number of consumers. Using wind power is not only depending on renewable source but also reduces the environmental impact of generating polluted greenhouse gases (including SO<sub>x</sub>, NO<sub>x</sub>, and mercury) and reduce the dependence on the fossil fuel. However, wind power technology still requires further research and innovation to improve turbine efficiency, life time, mitigate interconnection problems, power storage to smooth the power during short supply.

Renewable energy of wind and solar sources have a major drawback which requires comprehensive consideration in order to be used as a dependable standalone power generation source. The intermittent, unpredictable and variable rate of supply of both wind and solar make them unreliable power generation sources. The availability and the change in intensity of both sources around the day and the year are major problems and need to find a mechanism to store the abundant energy produced at the peak periods and use it at the short energy supply periods.

These fluctuations in power supply of renewable sources show the need of a storage system able to smooth the power generation during the variation of power supply from either of these two renewable sources.

The storage system solutions, in addition to smoothing the variable power generation of the renewable sources, also provide low greenhouse gas emissions, support voltage and grid frequency regulation, and reduce the amount of dispatching imposed on generators.

## 1.2 Energy Storage Technologies

Energy storage is a process of capturing an excess energy at a certain times and store it to be used when it is short or unavailable at different times. Energy comes in different forms mainly; electricity, chemical, radiation, electrical potential, high temperature, gravitational potential, mechanical, tidal, and kinetic. Energy storage usually converts energy of difficult to store forms, such as electrical, into storable forms. Energy storage technologies vary, some supply long-time storage and the others supply short-time storage. Pumped hydro energy currently accounts for 99% of the global bulk storage energy [4]

Lately, the grid electrical power has been mainly depending on burning fossil fuel which elevates the concern of air pollution, global warming and energy imports. This matter has evolved the use of renewable energy such as wind and solar power. However, one of the advantages of the fossil-fuel based electricity generation is the possibility to vary the power generation to fit the amount of used electricity. Unfortunately, that is not possible in the case of wind and solar power generation.

The wind power is uncontrolled in a sense that it is unavailable steadily all times. The intermittent wind power supply makes it unreliable source and effectively needs a storage backup to replenish the wind power shortage. The same issue occurs with the solar power which is only available mostly at day light with the disturbance of clouds.



Off grid electricity is becoming an effective market segment and is growing fast. An integrated reliable power source is always a need.

Generally, energy can be stored in wide range of forms, the following are the main and the most methods of energy storage whether they are natural, commercialized or not:

- Mechanical
  - Hydroelectricity dams
  - Pumped-storage hydroelectricity
  - Compressed air energy storage (CAES)
  - Flywheel energy storage
  - Gravitational potential energy
- Electrical
  - Capacitor
  - Superconducting magnetic energy storage (SMES)
- Electrochemical
  - Flow battery
  - Rechargeable battery
- Thermal
  - Brick storage heater
  - Cryogenic liquid air or nitrogen
  - Eutectic system
  - Ice storage air conditioning
  - Molten salt

- Phase Change Material
- Seasonal thermal energy storage
- Solar pond
- Steam accumulator
- Chemical
  - Biofuels
  - Hydrated salts
  - Hydrogen
  - Hydrogen peroxide
  - Power to gas
  - Vanadium pentoxide

Figure 1 highlights the leading commercialized power storage technologies:

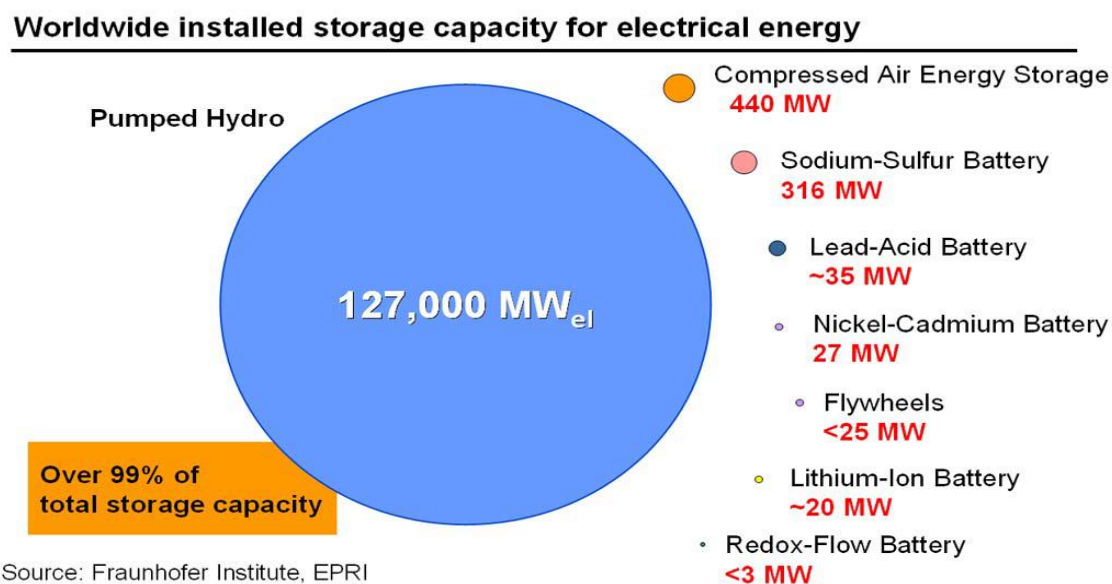


**Figure 1. Worldwide installed storage capacity for electrical energy (2010)**

### **Pumped-storage hydroelectricity**

Pumped-Hydro storage technology is considered the largest capacity of active energy storage, as Electric Power Research Institute (EPRI) [4] reports that PSH has 99% of bulk storage capacity share. The concept of this technology is to pump the water from lower level reservoir to higher level reservoir when there is an excess of generated electricity during lower peaks of demand. However, at times of higher demand the water at higher reservoir will be released through electricity generator turbine to supply the required higher demand.

### **Compressed air energy storage**

This technology uses surplus power at lower peak demand to compress air and store it in cavern or vessel. Once power is needed at higher demand, the air is heated, expanded and directed through power generator turbine. In addition to energy storage, this technology had been used in compressed air locomotive inside mines. Intensive development of this technology came up with a second generation (CAES) with higher efficiency and lower cost of consumed energy to heat and expand the compressed air. This technology is expected to have a growing trend in the energy storage industry.

### **Flywheel energy storage**

The concept of flywheel energy storage (FES) is to charge and store energy by accelerating a rotor to high speed and holding the energy by means of rotational energy. The rotor is connected to electrical generator which converts the kinetic energy into electricity. The generation of electricity discharges the stored rotational energy and

spinning speed declines, hence the FES needs to be recharged and increase its rotational speed. The flywheel is not intended to produce a large amount of energy and is considered a short duration energy storage. It is well known for its higher efficiency, longer life time and quicker response.

### **Lead Acid Batteries**

Lead-acid batteries are considered the most commercialized type of rechargeable batteries in the market. They have wide application including automotive, marine, telecommunication and many others. At the same time they have major limitations of their heavy weight and big volume. Their power output is not steady and consistent and their lifespan varies depending on the application. However, the continuous development of advanced lead-acid batteries is undergoing to improve its cycle life and durability, which will lead them to be properly used for peak shaving, frequency regulation, wind integration, and photovoltaic smoothing.

### **Sodium-Sulfur Batteries**

Sodium-sulfur batteries have the highest capacity among the commercial rechargeable energy storage batteries. They have applications in electric utility distribution grid support, wind power integration, and high value service applications. They are a molten-salt battery type, containing liquid sodium and sulfur. They have high energy density, high efficiency of charge/discharge and an approximate life time of 15 years. They are a registered trademark of the Japanese NGK Insulators Company. Around 316 MW NaS batteries have been installed globally and this number is expected to increase.

## **Nickel Cadmium Batteries**

Nickel-cadmium batteries are rechargeable type that uses nickel oxide hydroxide and cadmium as electrodes. Cadmium is a toxic element and the environmental impact of this type of batteries disposal has contributed significantly to the reduction of its use and production. In 1990, nickel cadmium batteries lost almost 80% of their market share. Recently, they were banned from most of the European Union countries and only can be supplied for replacement purposes or for certain types of new equipment. Presently, nickel-cadmium batteries have been replaced with nickel-metal hydride batteries.

A nickel-metal hydride batteries are also rechargeable and are similar to the nickel-cadmium batteries using the same positive electrode of nickel oxide hydroxide, but using hydrogen absorbing alloy instead of cadmium as the negative electrodes. A nickel-metal hydride battery can have two to three times the capacity of an equivalent size of nickel-cadmium type, and its energy density can approach that of a lithium-ion battery. In 2008, more than two million hybrid cars worldwide were manufactured with nickel-metal hydride batteries.

## **Lithium-ion Batteries**

Lithium-ion batteries are the most popular rechargeable type of batteries used mainly in electronic products. In Li-ion batteries the lithium ions transfer from the negative electrode to the positive electrode during discharge and return when charging. They have a high energy density, small memory effect and low self-discharge. Other than portable electronic, Li-ion batteries are becoming more popular with electric vehicles, aerospace and military applications, and even a replacement of the heavy weight lead

acid batteries. The high capacity and lower cost of Li-ion battery packs make them possible to be integrated into systems for grid support applications. Their higher energy density and lower weight make them an attractive choice for space constraint areas.

### **Vanadium Redox Flow Batteries**

Vanadium Redox Batteries (VRB) are a type of rechargeable flow batteries that use vanadium ions in different oxidation states to store chemical energy. Vanadium ions has the ability to exist in one solution in four different oxidation states. This unique property of vanadium makes it possible for VRB to use just one electroactive element instead of two, whereas all other types of flow batteries are storing the charge ions in two separate tanks of electrolytes, one of which stores electrolyte for positive electrode reaction while the other stores the electrolyte for the negative electrode reaction. Using one common electrolyte provides potential opportunity to increase cycle life of the battery.

For their relatively bulky size with other reasons, most vanadium batteries are used for grid energy storage application. They can be designed to provide energy of 2 to more than 8 hours, and their cell stacks lifespan is estimated to be around 15 years.

### **Power to Gas**

Power to gas (P2G) is one of the promising power storage technologies that converts electrical power to a hydrogen gas fuel. It can be deployed as power storage of wind and solar power generation stations. The surplus power or off-peak power generated by wind generators or solar arrays may then be used at a later time for load balancing of

electricity. The excess power is stored by means of hydrogen when using the power to electrolyze water into hydrogen and oxygen. Hence, stored hydrogen can be converted into power by utilizing one of three methods.

The first method is to inject the hydrogen into the natural gas grid or to be used in transport or industry. The second method is to combine the hydrogen with carbon dioxide and produce methane using a methanation reaction. The third method is to convert hydrogen to power (gas to power) using thermal engines, fuel cells or the BioGenerator which will be explained in later chapters. Figure 2 illustrates the concept of integrating power to gas storage with the renewable energy source.

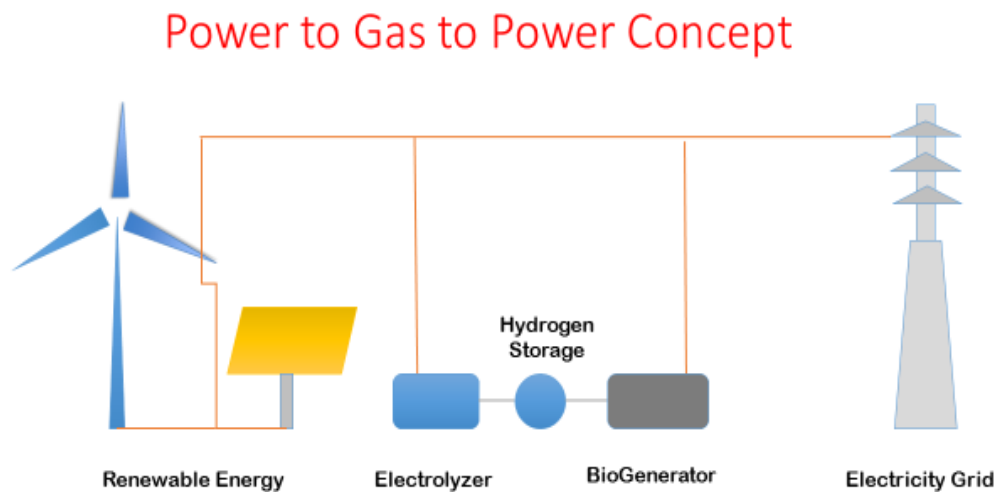


**Figure 2. Power to Gas (P2G) integrated with renewable energy**

## 1.3 References

- [1] Natural Resources Canada, <http://www.nrcan.gc.ca/home>
- [2] Canadian Wind Energy Association (CanWEA), <http://canwea.ca/>
- [3] Global Wind Energy Council (GWEC), <http://files.gwec.net/>, (Global Wind Energy Outlook 2016)
- [4] ELECTRIC POWER RESEARCH INSTITUTE, *A White Paper Primer on Applications, Costs, and Benefits* (Electricity Energy Storage Technology Options), 1020676, Technical Update, December 2010.



## Chapter 2

### 2 Literature Review

Recent technology advancement has put the power-to-gas as potential power storage option that can be integrated with the renewable power generation. In this method, excess or off-grid electricity is used to split water into hydrogen and oxygen by means of electrolysis. The produced hydrogen is stored and later can be used to generate power by different ways; it can be mixed with natural gas and burned in turbines, it can be combined with carbon dioxide to produce methane, or can be used directly for re-electrification using fuel cells.

#### 2.1 Fuel Cells Technology

The principle of fuel cell was invented in 1839 by the Welsh lawyer Sir William Robert Grove [5]. Sir W. Grove was examining the reverse process of water electrolysis by combining hydrogen and oxygen to produce water, before he noticed electricity generation due to this catalyzed by platinum reaction.

Fuel cell is simply a device that converts the chemical energy from a fuel into electricity through electrochemical reactions. In  $H_2/O_2$  fuel cells, hydrogen and oxygen are

combined producing electricity, heat, and water. Figure 3 shows the key system components of fuel cell for producing AC or DC power.

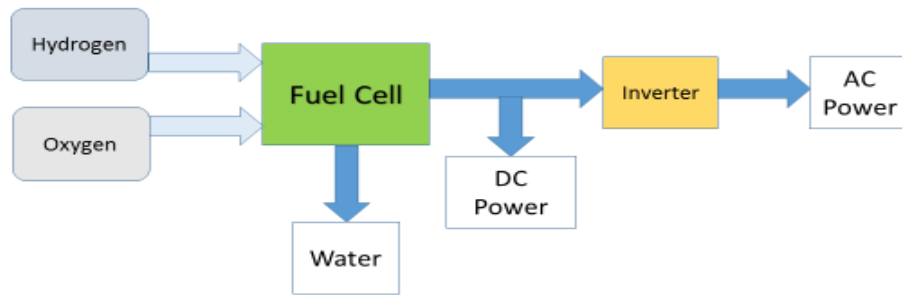


**Figure 3. Schematic diagram of fuel cell system key components.**

In general, the fuel cell is a battery, in which the fuel, oxidant and their product(s) are all fluids, and can be continuously fed or removed from/to the cell. Therefore, fuel cell works as long as it is fed with fuel and oxidant. Fuel cells can have quite a high energy conversion efficiency, up to 60%. Although fuel cells have great potential advantages, it was not until the 1950s in response to the needs of the US space program that practical devices were developed.

Though their basic principle looks simple, producing fuel cells as a practical product involves many engineering challenges and so far the proposed solutions are not cost effective. Even after several decades of research and development, today there is still no mass production of fuel cells and the currently produced fuel cells are used for limited

applications, while some major production is used for research and development labs over the world.

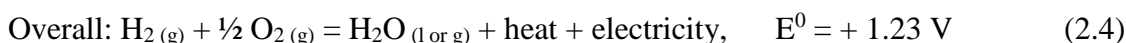
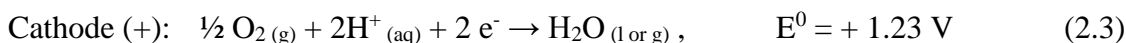
Fuel cells are different from combustion engines, as they work on the “cold combustion” principle. There are several different types of fuel cells, they differ in their fuels, operating temperature and other conditions. They use relatively highly efficient electrochemical processes and don't cause mechanical wear and tear to their components.

The most popular type of fuel cells is the proton exchange membrane (PEM) fuel cell also called the polymer electrolyte membrane fuel cell. It uses hydrogen as the fuel and oxygen usually from air as the oxidant.

The overall PEM fuel cell reaction is:



The fuel cell consists of two electrodes; anode and cathode, separated by a polymer electrolyte membrane allowing only protons to pass through and get transferred from the anode to the cathode. Two different half reactions occur in the fuel cell, each of the half reactions occurs at different electrode of the fuel cell, both reactions comprise the overall reaction and produce electricity and heat, as shown in equations 2.2, 2.3 and 2.4:



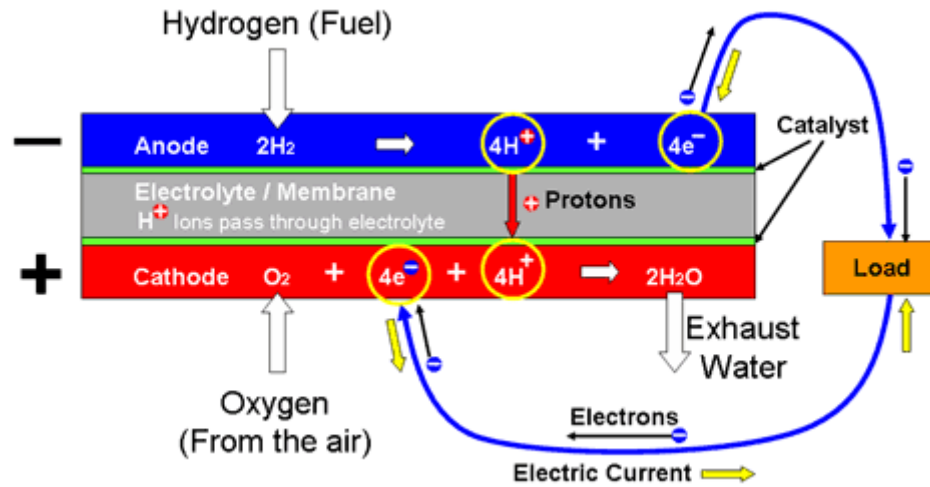


**Figure 4. Fuel Cell Electrochemistry**

Figure 4 illustrates the fuel cell half reactions at the individual electrodes. The electrodes are made from porous carbon which allows the active gases to pass through and the electrode surfaces are inked with platinum catalyst to accelerate the reactions. The electrolyte is a thin sheet of cation ion exchange polymer about 50 microns thick which permits the passage of hydrogen ions and doesn't conduct electrons.

As shown in Figure 4 and reaction 2.2, the hydrogen is oxidized at the anode and loses its electron in the process. The proton (the positive hydrogen ion) passes through the electrolyte membrane to the cathode while the electron travels around the external circuit to the cathode.

The oxygen which is supplied to the cathode, is reduced by reacting with the electrons and with hydrogen ions, both coming from the anode, to form water (reaction 2.3). The

electrons travel from the anode to the cathode via external circuit represent the conventional electrical current flowing in the opposite direction.

The rate of oxidation at the anode and the rate of reduction at the cathode in some types of fuel cells are very slow, therefore, catalysts are used to increase the rate of these reactions at lower temperatures. Alternatively to avoid the cost of expensive catalysts, some fuel cells are designed to operate at higher temperatures. In PEM and some other fuel cells, platinum catalyst is used. Unfortunately, it is very expensive and sensitive to poisoning by very small amounts of carbon monoxide, which requires additional purification processes to eliminate potential contamination from the system.

Single  $H_2/O_2$  fuel cell usually produces low voltage (0.6-0.7 Volt) which means that the system needs a certain number of cells connected in series (a stack) to obtain the required voltage. Therefore, the potential generated power can be obtained by assembling different number and size of individual fuel cells to comprise the stack and the surface area of the unit. Figure 5 illustrates the configuration of fuel cell stack with multiple cells.

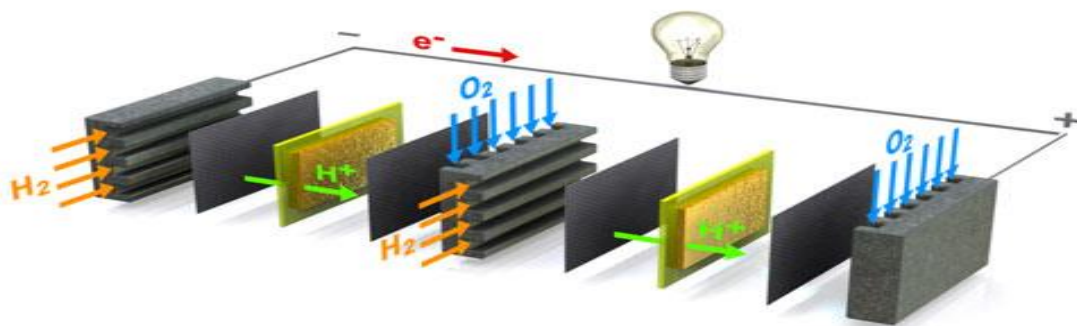


**Figure 5. The configuration of fuel cell stack with multiple of single fuel cell components**

## 2.2 Fuel Cell Types

Basic fuel cell operation has many challenges which led the researchers to come up with range of fuel cell designs using different basic chemistry. These fuel cell types have been developed to meet different design or operating criteria such as less expensive construction, more efficient fuel utilization, faster start-ups or the use of more convenient or less expensive fuels. Higher power outputs can be achieved by operating at higher temperatures, by using catalysts to accelerate the fuel cell electrochemical reactions and by using electrodes with a greater surface area.

### 2.2.1 Conventional Fuel Cells

Currently there are six major fuel cell types being developed for different applications. Some of these fuel cells operate at high temperatures and some use unique electrode materials or catalysts:

- Proton Exchange Membrane Fuel Cell
  
- Alkaline Fuel Cell
  
- Phosphoric Acid Fuel Cell
  
- Molten Carbonate Fuel Cell
  
- Solid Oxide Fuel Cell
  
- Direct Methanol Fuel Cell

These fuel cells have been proposed for a wide range of applications from powering laptop computers, through automotive transportation to high power load levelling.

### Proton Exchange Membrane Fuel Cell

Proton exchange membrane (PEM) fuel cells need hydrogen and oxygen from the air to operate. They use solid polymer as an electrolyte and porous carbon electrodes containing platinum or platinum alloy catalyst. As illustrated in Figure 6, the hydrogen gas is oxidized on the anode splitting into a proton and electron, only the proton passes through the polymer electrolyte membrane from the anode to the cathode. The electron travels through external electrical loop from the anode to the cathode generating the electrical current. At the cathode the migrated proton along with the electron reduce the oxygen to water forming the overall reaction product and generating electricity and heat. PEM fuel cells deliver high power density and have the advantages of low weight and volume compared with other fuel cells. They are typically fueled with pure hydrogen.

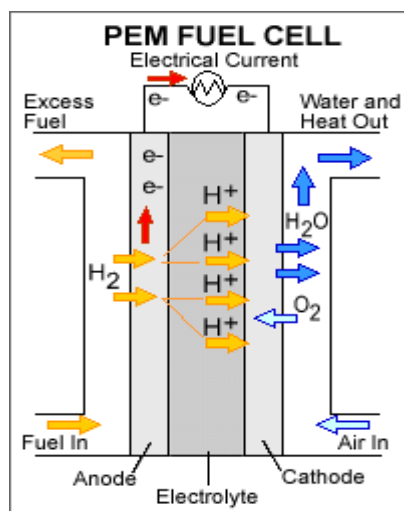


Figure 6. Basic structure and processes in PEM fuel cell, <https://energy.gov/>

PEM fuel cells operate at relatively low temperatures, around 80°C (176°F), cold start below 0°C is also proven. Low temperature operation allows them for quick start (less warm-up time) and leads to less wear on system components hence better durability. However, a noble-metal catalyst (typically platinum) is required as an electrocatalyst at both electrodes to accelerate the rate of both half reactions, the use of expensive metal results in high cost of the system. Moreover, the platinum catalyst is extremely sensitive to carbon monoxide poisoning, which entails the necessity of employing an additional unit to remove carbon monoxide from the fuel gas if the hydrogen is derived from a hydrocarbon fuel, which means another cost increment.

However, PEM fuel cells have a good combination of efficiency, power output and low operating temperature make them among other types, the best choice for automotive applications. Currently, PEM fuel cells are used primarily for transportation applications and some stationary applications. Due to their fast start-up time and favorable power-to-weight ratio, PEM fuel cells are particularly suitable for use in passenger vehicles, such as cars and buses. The rated power density of the PEMFC of 0.7 W.cm<sup>-2</sup> and higher is attainable depending on operating conditions.

### **Alkaline Fuel Cell**

Alkaline Fuel Cells (AFC) need oxygen from the air and hydrogen to operate as in the case of PEM fuel cells. They use aqueous solution of potassium hydroxide as an electrolyte. Figure 7 illustrates the basic structure and processes in the AFC. The operating temperature is usually around 80°C, but can be as high as 200°C, at higher pressure. The power density of the AFC is in the range of 0.1 – 0.3 W.cm<sup>-2</sup>.



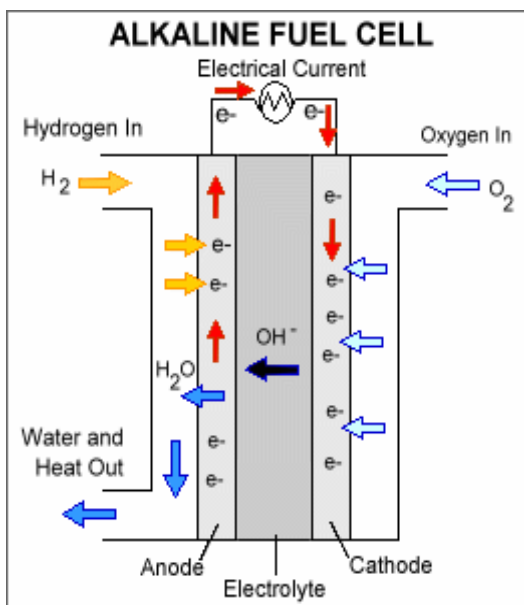


**Figure 7. The basic structure and processes in AFC, <https://energy.gov/>.**

They were some of the earliest practical fuel cells and were used in the US space program for producing drinking water and generating electricity on-board of spacecraft. AFCs are usually not using platinum catalyst on their electrodes, but instead they use a variety of non-precious metals as a catalyst at the anode and cathode. Therefore, they are less expensive compared with PEM cells and have a relatively high operating efficiencies of 60%. Unfortunately conventional AFCs are facing many challenges affecting their performance, reducing their power output and shortening their lifetime such as shunt currents, wettability, corrosion, difficulty in handling differential pressure across the electrolyte. The most important challenge for this fuel cell type is that it is susceptible to poisoning by carbon dioxide. In fact, even a very small amount of CO<sub>2</sub> in the air can dramatically affects cell performance and durability due to carbonate formation in the electrolyte.

To overcome the challenges of conventional AFC, recently a novel AFC that uses a polymer membrane as the electrolyte instead of potassium hydroxide liquid has been developed. It is closely related to conventional PEM fuel cell, except that they use an alkaline membrane instead of an acid membrane.

Alkaline membrane fuel cells (AMFCs) address some of these concerns and have lower susceptibility to CO<sub>2</sub> poisoning compared with liquid-electrolyte AFCs. However, CO<sub>2</sub> still affects performance of AMFCs, and performance and durability of the AMFC are still lower than that of PEMFCs. AMFCs still have challenges including tolerance to carbon dioxide, membrane conductivity and durability, higher temperature operation, water management, power density, and anode electro-catalysis.

### **Phosphoric Acid Fuel Cell**

Phosphoric Acid Fuel Cells (PAFC) also need hydrogen and oxygen from the air to operate. PAFCs use phosphoric acid as an electrolyte, the acid is contained in a Teflon-bonded silicon carbide matrix and both electrodes, anode and cathode, are made of porous carbon containing platinum catalyst. The basic structure and the electrochemical reactions that take place in the cell are shown in Figure 8.

They run at high temperatures of around 220°C and can deliver high power of a Megawatt range but have relatively low efficiency of around 37-42%. The power density of the PAFC is in the range of 0.14 W.cm<sup>-2</sup>. However, due to the poor conversion efficiency it causes significant heat generation in the fuel cell stack. This excess heat can

be recovered using combined heat and power (CHP) applications, hence improving the system efficiency.

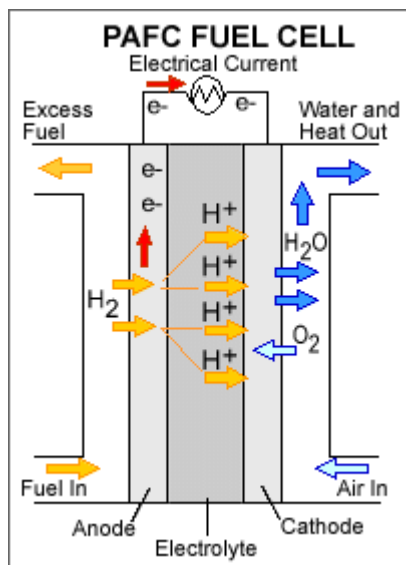


**Figure 8. The basic structure and processes in PAFC, <https://energy.gov/>.**

The PAFC is always considered the first generation of modern fuel cells. This type of fuel cell is typically used for stationary power generation, but some PAFCs have been used to empower large vehicles such as city buses.

Compared with PEM fuel cells, PAFCs are considered more tolerant to impurities which come with hydrogen when reforming fossil fuels. Although PAFCs are more than 85% efficient when used for the co-generation of electricity and heat, they are less efficient at generating electricity alone (37%–42%). So, when compared with other fuel cells, PAFCs are considered less powerful than others, having the same weight and volume. As a result, PAFCs are not only large and heavy but are also expensive. They require much higher loadings of expensive platinum catalyst than other types of fuel cells do, which raises their cost.

## **Molten Carbonate Fuel Cell**

Molten Carbonate Fuel Cells (MCFC) also need hydrogen and oxygen to operate. MCFCs are high temperature fuel cells that use an electrolyte composed of a molten carbonate salt mixture soaked in a porous, chemically inert ceramic lithium aluminum oxide matrix. MCFCs run at higher temperatures of 650°C to 1000°C. Because they operate at high temperature, no precious metals are used as catalysts at the anode and cathode. Their achieved efficiencies can reach 45% or more and power outputs of over 1 Megawatt are typical in grid supply applications. The power density of the MCFC is in the range of 0.1 – 0.12 W.cm<sup>-2</sup>. The basic structure and the electro-chemical reactions that take place in the MCFC are shown in Figure 9.

Under the high temperatures at which MCFCs operate, methane and other hydrocarbons are internally reformed inside the fuel cell and converted into hydrogen and carbon dioxide, so there is no need for external reforming process to supply the fuel cell with pure hydrogen as in the cases of alkaline, phosphoric acid and PEM fuel cells. This shortcut process results in a major reduction of MCFCs cost when compared with other fuel cell types. MCFCs are currently under development to be fueled by natural gas and coal for use in power plants, various industries and military applications.

MCFCs have improved efficiency over PAFCs. They can reach 65% efficiencies when coupled with a turbine, and when capture and use the wasted heat, overall fuel efficiencies can reach 85%.

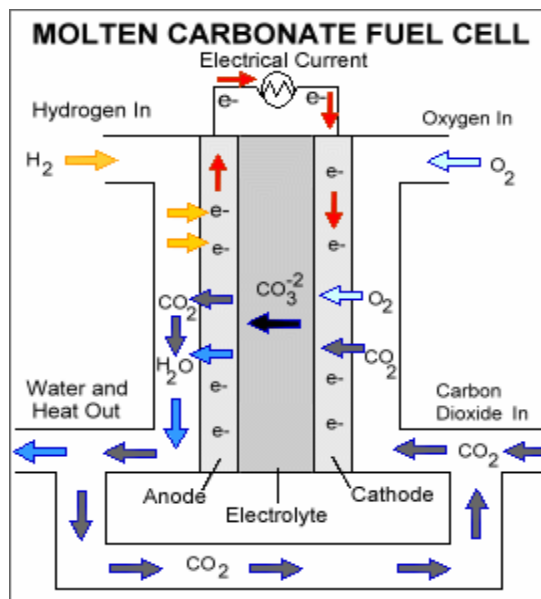


**Figure 9. The basic structure and processes in MCFC, <https://energy.gov/>.**

While the high temperature operation of MCFCs have the advantage of eliminating the external reforming process, their disadvantages include the reduced durability of the MCFCs, along with the highly corrosive nature of the electrolyte, both of which decrease the fuel cell life time. However, extensive studies are exploring corrosion resistant materials and fuel cell designs that improve the performance and prolong the cell lifetime.

### **Solid Oxide Fuel Cell**

Solid Oxide Fuel Cells (SOFC) need hydrogen and oxygen from the air to operate. SOFCs also operate in the same or even higher temperature range as the MCFCs (800 to 1,000°C). They use a rigid, non-porous ceramic compound as an electrolyte which can stay solid at high operating temperatures. SOFCs can deliver power of several Megawatts but at an efficiency around 60% at converting fuel to electricity. However,

when the system's waste heat can be utilized (co-generation), the overall fuel efficiency can reach 85%. The power density of the SOFC is in the range of  $0.15 - 0.7 \text{ W.cm}^{-2}$ . The basic structure and the electro-chemical reactions that take place in the SOFC are shown in Figure 10.

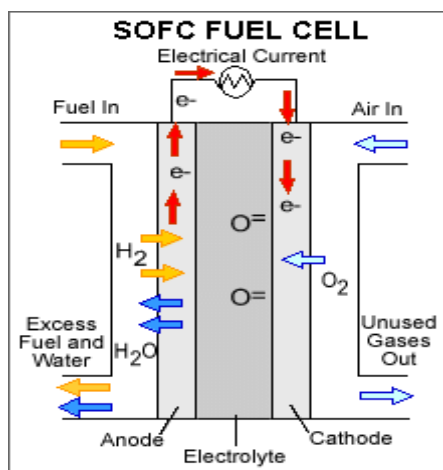


**Figure 10. The basic structure and processes of the SOFC, <https://energy.gov/>.**

Since the SOFCs operate at very high temperatures, they have the advantage of not using precious metal catalyst at the electrodes. As in the case of MCFCs, the high temperatures at which SOFCs operate, allows SOFCs to reform a variety of fuels internally inside the fuel cell, eliminating the need of external reforming. This would also result in the major reduction of the cell and operation costs.

SOFCs are the most sulfur-resistant fuel cell type; they are also not poisoned by carbon monoxide. This feature allows SOFCs to use different types of fuels like natural gas, biogas, and gases produced from coal and organics gasification. As in the case of MCFCs, the high temperature operation has also disadvantages. It causes a slow start-ups and requires special shielding to retain heat and protect personnel, which may limit their

applications to utility power generation and not for transportation. The high operating temperatures also affect negatively the durability of the cell and development of low cost materials with higher durability is a technical challenge for this technology.

### Direct Methanol Fuel Cell

Direct Methanol Fuel Cells (DMFC) are similar to PEM cells but they use methanol instead of pure hydrogen and oxygen from the air to operate. They work at low temperatures of 50°C to 100 °C. Maximum obtained power densities are around 0.25 W.cm<sup>-2</sup>. All other types of fuel cells are powered by hydrogen whether it is fed directly or generated inside the fuel cell by internal reforming of hydrogen of fuels such as hydrocarbon fuels. However, DMFCs are powered by pure methanol which is usually mixed with water and fed directly to the anode side of the fuel cell. Using such inexpensive liquid fuel avoids both the hydrogen supply challenges and the requirement of external or internal reformer. The basic structure and the electro-chemical reactions that take place in the DMFC are shown in Figure 11.

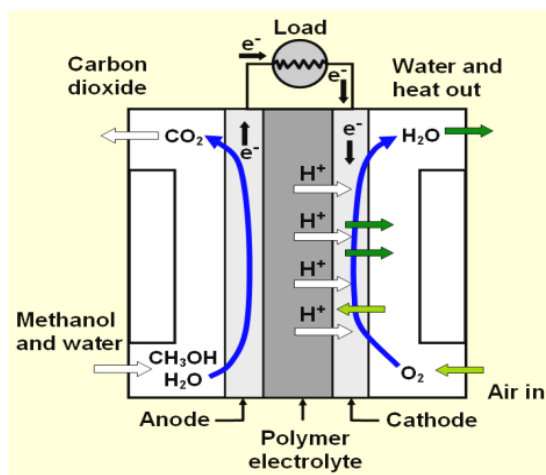


Figure 11. The basic structure and processes of the DMFC, [www.intechopen.com](http://www.intechopen.com).

Methanol has a higher volumetric energy density than hydrogen and since it is in the liquid form at ambient temperatures, makes it much easier to be transported and stored compared with the gas fuels used in other fuel cells. DMFCs are mostly used for low power applications such as portable electronics.

Table 1 classifies the different types of fuel cells based on their operating temperatures, type of fuel and used electrolyte.

**Table 1. Classification of Fuel cells based on operating temperatures, used fuels and electrolytes**

	Operating Temp. (°C)	Fuel	Electrolyte
<b>PEMFC</b>	40-90	H <sub>2</sub>	Polymer
<b>AFC</b>	40-200	H <sub>2</sub>	KOH
<b>PAFC</b>	200	H <sub>2</sub>	Phosphoric Acid
<b>MCFC</b>	650	CH <sub>4</sub> ,H <sub>2</sub>	Molten Carbonate
<b>SOFC</b>	600-950	CH <sub>4</sub> ,H <sub>2</sub>	Solid Oxide
<b>DMFC</b>	60-130	Methanol	Polymer
	<b>Noble metals</b>	<b>Noble/non-noble</b>	<b>Non-noble</b>



## 2.2.2 Biological Fuel Cells

Biological fuel cells have been investigated since it was discovered that many biological pathways have bio-electrochemical side, which proved that biological reaction may induce an electrical action [6].

There are different biological mechanisms that can be utilized to operate biological fuel cells, including:

- 1- Microbial cells that deploy biochemical path to convert a primary organic fuel into a secondary fuel such as hydrogen or ethanol. This biological process can be used within a conventional fuel cell to supply it with its fuel [6].
- 2- Microbial cells that convert chemical energy directly into electrical energy by oxidizing an organic fuel (i.e. glucose) using proteins, enzymes or microorganisms. The generation of power is directly by biological means [7 and 6].
- 3- Microbial cells that combine both the utilization of photo-chemically active and biological systems to collect the energy from sunlight and convert it into electrical energy [8, 9 and 10].

In general, biological fuel cells can convert the energy of the biochemical oxidation of organic or inorganic substrates directly into electrical energy, allowing to generate electricity from electro-chemically passive compounds [11].

The biological and chemical fuel cells have similar basic principles. The biological fuel cell comprises of two chambers, one containing the anode and the other containing the

cathode. The biocatalyst at the anaerobic anodic chamber could be either enzyme or whole microbial cell. This biocatalyst oxidizes the fuel which could be organic matter producing electrons and protons. These protons migrate through a selective membrane (electrolyte) separating the anodic from the cathodic chambers which allows the protons only to pass through to the cathode. The electrons travel via an external circuit loop connecting the anode with the cathode generating the electrical current. At the cathode the electrons and the protons combine with the oxygen to form water [12]. Figure 12 illustrates the components of the microbial fuel cell.

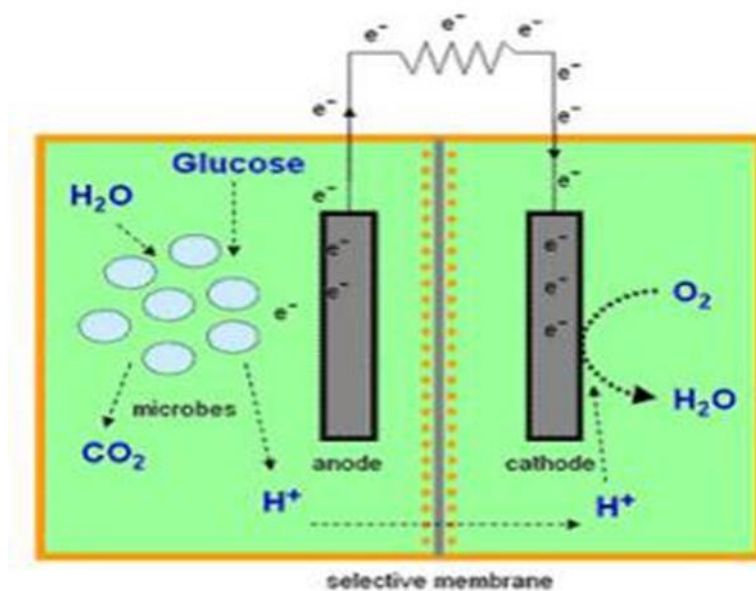


**Figure 12. Schematic representation of a typical MFC, <https://biologicalfuelcell.com/>**

The biological fuel cells can be also classified into two main types based on the used biocatalyst - enzymes or whole microbial cells. Enzyme biocatalysts are expected to increase the conversion rate of substrate, to facilitate the maintenance of the set, and to stabilize the parameters of the biofuel cell. However, the use of microbial biocatalysts (in

the case of microbial fuel cells, MFC) is preferable to enzymes, because of their specific features. Microorganisms oxidize wide range of substrates so they can be used with various organic fuels, and they are not easily poisoned and lose their activity under normal operation conditions as in the case of enzymes. Furthermore, the cost of microorganisms is much lower than of enzymes as the latter require special production and purification manufacturing processes [13].

Nevertheless, In the case of microbial fuel cells, microorganisms play a significant role as they are responsible for the bioconversion of the fuel by splitting it into protons and electrons; they also can contribute to the electrons transfer to the anode. There have been many studies that focus in using microbial cells in the fuel cell to oxidize the fuel in the anode and to catalyze the reduction of oxygen in the cathode [7].

A variety of microorganisms, both axenic (pure) and mixed cultures of anaerobic or facultative species are currently used as biocatalysts in microbial fuel cells. The mixed cultures are preferable to the axenic ones due to their important advantages. Mixed cultures have a higher resistance against process disturbances, larger substrate versatility and a higher power output [13].

According to thermodynamics, the maximum voltage generated by a single MFC is around 1V, while the practically obtained maximum voltage is 0.8V. In order to obtain higher voltages, the cells have to be arranged in series (stacks). The reported so far current generated by MFCs has not exceeded 0.1A. The average power density of a single MFC is around 40 W/m<sup>3</sup>. Recently, stacked configurations of several MFCs have reached

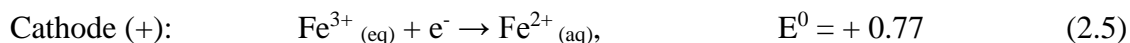
power densities of  $250 \text{ W/m}^3$ , implying that improvements in MFC performance are under way.

However, despite the great advancement in recent years in this research field, MFCs are still suffering significant hurdles for their large scale implementations. The major obstacles are due to the insufficient performance with both anodic and cathodic electron transfer, upscale technical issues and high investment costs.

## 2.3 BioGenerator

The BioGenerator is a unique invention meant to generate electricity by converting chemical energy hydrogen oxidation into electrical energy. It uses to a certain degree the concept of PEM fuel cell, as they share the same anodic reaction of oxidizing the hydrogen gas into protons and electrons, equation 2.2. The protons as in the case of PEMFC migrate through a selective membrane (i.e. proton exchange membrane) from the anodic chamber to the cathodic chamber.

However, the cathodic reaction of the BioGenerator is different from the one of PEMFC. In the BioGenerator on the cathode, the ferric iron ( $\text{Fe}^{3+}$ ) is reduced to ferrous iron ( $\text{Fe}^{2+}$ ) by receiving the electrons produced at the anode which travel via external loop from the anode to the cathode generating the electrical current, the BioGenerator cathodic reaction is expressed as:



By comparing the above cathodic reaction of the BioGenerator with the one of other fuel cells, the BioGenerator is not similar to any of the six conventional fuel cell types that mentioned in the previous section, and neither to the known microbial fuel cells.

Technically, the BioGenerator is comprised of two main parts; electrochemical stack and bioreactor.

The electrochemical stack is a unit that has the same concept as the fuel cell. It has two electrodes (i.e. anode and cathode) separated by selective proton exchange membrane. Both electrodes are made of porous carbon material and the proton exchange membrane has the same function of the one of PEM fuel cell.

In order to generate continuous power supply, both hydrogen gas and ferric iron in aqueous solution have to be continuously fed to the electrochemical stack unit to assure both anodic and cathodic half reactions are continuously progressed and the electrons are continuously flowing from the anode to the cathode generating electrical current.

At the cathode as shown in equation 2.5, the ferric iron is continuously reduced to ferrous iron and in order to feed the electrochemical stack with continuous supply of ferric iron aqueous solution, the ferrous iron has to be oxidized to ferric iron. This process is accomplished biologically in a separate bioreactor which is the second main part of the BioGenerator. Figure 13 illustrates the schematic diagram of the BioGenerator.

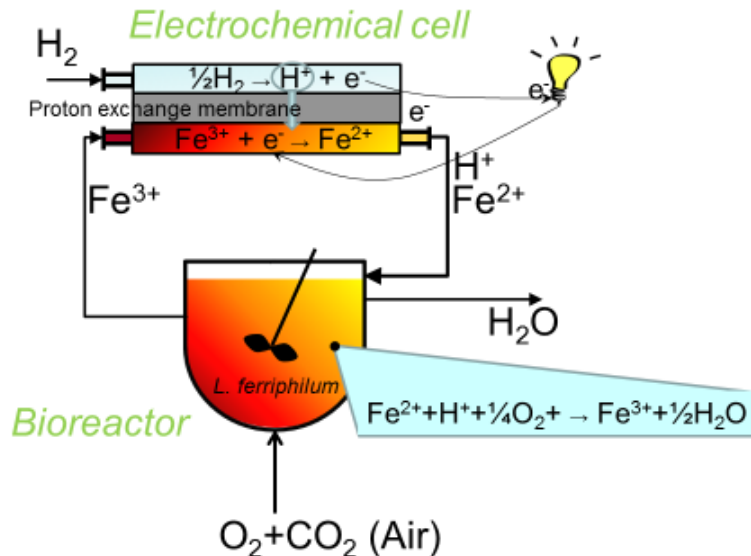


**Figure 13. Schematic diagram of the BioGenerator**

In the bioreactor, the actual and complete half cathodic reaction takes place. Ferrous iron bio-oxidizing microbial culture is mobilized in the bioreactor as either attached or suspended culture. The function of this microorganisms is to oxidize the ferrous iron into ferric iron, so the liquid medium in the bioreactor which contains high concentrations of ferric iron as an aqueous solution is pumped to the cathodic chamber of the BioGenerator's electrochemical stack unit. The aqueous solution of ferrous iron and protons that passed through proton exchange membrane from the anodic chamber to the cathodic chamber, are then returned to the bioreactor. The bioreactor is also supplied with air from which the dissolved oxygen reacts with protons completing the cathodic half reaction as shown in the following equation:



After combining reactions 2.2 and 2.6, the overall net reaction in the BioGenerator is:



Most of the energy of hydrogen oxidation ( $Q=142 \text{ MJ / kg}$ ) is converted to electrical energy. In addition, approx. 30% of the energy of reaction 2.6 is released as waste heat, while 7% is used by microorganisms for microbial growth and maintenance.

The main role of the bioreactor is to transfer the chemical energy of oxygen to ferric ions (reaction 2.6) by re-oxidizing ferrous to ferric iron.

The rate of reduction of ferric iron at the cathode (2.5), which under steady state conditions is equal to the rate of ferrous iron oxidation in the bioreactor (2.6) are both proportional to the electrical current (i.e. the rate of flow of electrons shuttled between reactions 2.2 and 2.5) drawn from the BioGenerator.

Ferrous iron oxidizing microorganisms (IOM) are class of microorganisms which in nature are responsible for the formation of acid mine drainage. IOMs are mainly autotrophic and mixotrophic types of bacteria which live in media having wide range of temperatures, reaching  $50^{\circ}\text{C}$  and a pH as low as zero. These different types of bacteria oxidize ferrous iron into ferric iron. They are mainly autotrophic, use carbon dioxide as the carbon source and oxygen as the electron acceptor.

The main iron oxidizing microorganisms are *Thiobacillus ferrooxidans*, *Leptospirillum ferriphilum*, and *Cyanidium caldarium*. Each of these species dominate at certain optimum media temperature and pH, also each of these species have different iron oxidation rates, as the highest one attributed to *Leptospirillum ferriphilum*. The optimum

growth of *Leptospirillum ferriphilum* occurs at 40-45<sup>0</sup>C and pH 0.7-1.5 [9]. Different types of bioreactors can be used in the BioGenerator, where the airlift was used initially for the bench scale and later for the pilot plant BioGenerator. Later a trickling bed bioreactor was used as bench scale for some test studies.

In both bioreactor types, close to optimum microbial culture growth conditions need to be maintained. The bioreactor temperature has to be kept at 40-45<sup>0</sup>C and the pH at 0.7 to 1.2. In the case of airlift bioreactor which relies on bubbling air supply, adequate air flow rate has to be maintained to assure that the required amount of oxygen according to equation 2.6 has been transferred to the bioreactor liquid. Oxygen mass transfer is usually the limiting factor of the power generation in the entire BioGenerator. Nevertheless, in the case of trickling bed bioreactor which relies on circulating the bioreactor liquid to diffuse the oxygen from the atmosphere, all mass transfer parameters should be considered while calculating the circulation flow rate to assure the exact required oxygen quantity has been dissolved in the bioreactor liquid.

## 2.4 BioGenerator Challenges

As any emerging technology, BioGenerator has many areas that need further investigation and development to reach commercial stage.

As previously mentioned the BioGenerator comprises of two main components; electrochemical stack and bioreactor. The electrochemical stack of the BioGenerator



continuously receives bioreactor liquid with pH in the range of 0.7 to 0.9 and temperature of around 40°C, this liquid contains high concentration of ferric ions that can reach 50 g/L.

One of the by-products of the microbial iron oxidation is jarosite [10], which is an insoluble basic that can plug the pores of the cathode. Therefore, the minimization of jarosite formation is highly desired. The complete elimination of the jarosite formation can be achieved by bringing the pH in the bioreactor to below 0.9.

The other main element of the BioGenerator is the bioreactor. Supplying the required amount of oxygen is the most important power consumption element in the BioGenerator. In order to increase the electricity output of the BioGenerator, higher concentration and flow rate of ferric ions have to pass through the electrochemical stack unit and the reduced ferric ions into ferrous ions in the cathodic chamber are delivered to the bioreactor to be biologically re-oxidized once again into ferric ions. From the stoichiometric relationship of equation (2.6), 1 g of oxygen is needed to react with 7.4 g of ferrous ions which when calculating the actual oxygen transfer rate (AOTR) turns to huge amount of oxygen needed to be transferred to the bioreactor liquid. Reducing the required amount of air to transfer the same amount of oxygen is a very important factor to reduce the operational cost of the BioGenerator and increase the energy efficiency of the amount of generated electricity compared to the amount of consumed electricity. Improving the oxygen transfer rate and reducing the running cost of the BioGenerator leads us to investigate different types of bioreactor designs and configurations. This was the main reason of researching the dynamics of trickling bed bioreactor type and compare its performance to the initially used type “Airlift” bioreactor. In addition to the bioreactor

design, there are many other parameters that can improve the oxygen transfer efficiency, just like the type of air diffuser used, the depth of the liquid inside the bioreactor, and the temperature of the liquid.

Ferrous iron oxidation rate is another main factor that can play major role in reducing the volume of the bioreactor and the capacity and size of the auxiliary equipment, piping and fittings required for the process. More studies need to be conducted on various iron oxidizing species by varying the reaction parameters and study their effects on ferrous iron oxidation rate.

Furthermore, an economical studies are also needed to give more factual idea of both capital and operational costs of large scale BioGenerator for commercial comparison with other power storage options. However, this study was conducted and presented in chapter 4 in this thesis.

## 2.5 References

- [1] Webb, K. R. "Sir William Robert Grove, (1811-1896) and the origins of the fuel cell." *Journal of the Royal Institute of Chemistry* 85 (1961) 291-293.
- [2] F. Davis, S. P. J. Higson, Biofuel cells—Recent advances and applications. *Biosensors and Bioelectronics* 22 (2007) 1224–1235
- [3] R.A. Bullen, T.C. Arnot, J.B. Lakemanc, F.C. Walsh, Biofuel cells and their development, *Biosensors and Bioelectronics* 21 (2006) 2015–2045
- [4] T. Yagishita, S. Sawayama, K. Tuskahara and T. Ogi, Effects of intensity of incident light and concentrations of *Synechococcus* and 2-Hydroxy -1, 4-Naphthoquinone on the current output of photosynthetic electrochemical cell, *Solar Energy* Vol. 61, No. 5, (1997) pp. 347–353.
- [5] S. Tsujimura, A. Wadano, K. Kano, T. Ikeda, Photosynthetic bio-electrochemical cell utilizing cyanobacteria and water-generating oxidase, *Enzyme and Microbial Technology* 29 (2001) 225–231.
- [6] Linda de la Garza, G. Jeong, P. A. Liddell, T. Sotomura, T. A. Moore, A. L. Moore, and D. Gust, Enzyme-Based Photo-electrochemical Biofuel Cell, *The Journal of Physical Chemistry B* 107 (2003), 10252-10260.
- [7] Varfolomeev, S.D., Krylova, L. & Zaikov, G.E. (eds) 2008, *Molecular and nanoscale systems for energy conversion*, Nova Science Publishers, Inc.

- [8] A.K. Shukla, P. Suresh, S. Berchmans and A. Rajendran, Biological fuel cells and their applications, *Current Science*, Vol. 87, No. 4 ( 2004), P 14.
- [9] K. Penev. D. Karamanev, Batch kinetics of ferrous iron oxidation by *Leptospirillum ferriphilum* at moderate to high total iron concentration, *Biochemical Engineering Journal*, Volume 50, Issues 1–2, (2010) 54–62
- [10] J. Daoud, D. Karamanev, Formation of jarosite during  $\text{Fe}^{2+}$  oxidation by *Acidithiobacillus ferrooxidans*, *Mineral Eng.*, 19 (2006), pp. 960-967

## Chapter 3

# 3 Study of the Dynamics of Ferrous Iron Biooxidation by *Leptospirillum ferriphilum* in a Trickle Bed Bioreactor Used for Energy Storage

## 3.1 Introduction

The use of energy storage technologies is probably the best way to solve the problem of power variability. One of the most promising ways to store electrical energy is based on the use of hydrogen as an intermediate storable energy vector. The hydrogen-based energy storage contains three main components: electrolysis of water during a peak renewable power generation, storage of the produced hydrogen, and re-electrification of the stored H<sub>2</sub> back to electricity during a low renewable power generation. While both the water electrolysis and hydrogen storage are relatively well developed, there is currently no reliable commercial technology for the re-electrification of hydrogen, i.e. for the conversion of hydrogen to electricity. The recently invented technology named BioGenerator [1] is a unique, commercially-viable electro-bio-chemical process for the conversion of hydrogen to electricity, as explained in the previous section 2.3.

In the hydrogen-based energy storage, the convertor of hydrogen to electricity is turned on mostly during the periods of reduced wind or solar power generation or of their complete absence. Therefore, the BioGenerator, and its bioreactor, are operational during

the low wind or solar power generation, while they are idle during high renewable power generation (sunny and/or windy periods). Figure 14, illustrates the sequential time profile of the BioGenerator operation.

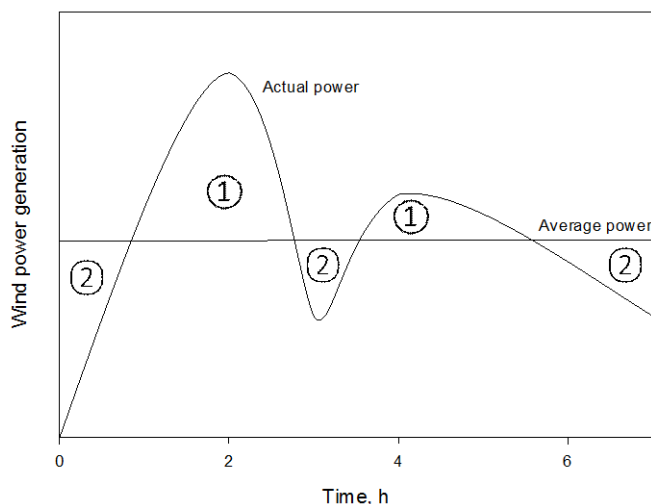


**Figure 14. Typical time profile of wind power generation and smoothing to its average value.**

1 – Excess wind generation: electrolyzer on, BioGenerator off; 2 – low wind power generation: electrolyzer off, BioGenerator on.

Trickling bed bioreactor is a type of bioreactors considered to be used in the BioGenerator for its beneficial characteristics compared to other bioreactor types. The main advantage of trickling filters is the low energy consumption and high oxygen transfer rate.

The main idea of trickling bed bioreactor is circulating the bioreactor solution liquor to assure dissolving the required oxygen for iron oxidation reaction and growth of microorganisms. This mechanism avoids the usage of air blowers for aerating the

bioreactor and in the same time increases the residence time inside the bioreactor tending for higher iron oxidation rates.

The main aim of this work is to study the bioreactor behavior during and after interruptions of the substrate (ferrous iron) delivery. The main question to be answered whether the microbial activity is influenced by interruptions in the substrate supply, which is expected during the operation of the bioreactor as part of the BioGenerator.

## 3.2 Materials and Methods

### 3.2.1 Description of Experimental Setup

The experimental setup used in this work is shown in Figure 15. The experiments were performed using two trickling bed bioreactors with a shape of vertical cylinders. They had an internal diameters of 9 cm and a total height of 70 cm. Each of the bioreactors has a perforated plastic plate (8 cm holes) fixed at 6.6 cm above the bottom of the bioreactor. Above the plate, the bioreactors were separated by a vertical plexi-glass plate (30 cm high) into two equal compartments. One of these compartments was filled with plastic biofilm support.

The liquid medium, trickling over the plastic support, was collected below the perforated plate. The volume of liquid below the plate was maintained at approximately 0.410 L. The liquid medium was distributed over the trickling medium by using a peristaltic pump

(Thermo Fisher Scientific, model 7523-70) which was drawing liquid from the space below the perforated plate. The flow rate of the circulating liquid was 100 mL/min. A second peristaltic pump (Thermo Fisher Scientific, model no. 7521-50) was used to provide each bioreactor with feed solution containing ferrous sulfate and a nutrient solution (9K) with feed rate of 0.4 mL/min. A second channel of the same pump was used to withdraw the spent solution from the bioreactors by means of a fixed drain suction tube installed on top level of the liquid under the perforated plate. The feeding rate was higher than the evaporation rate.

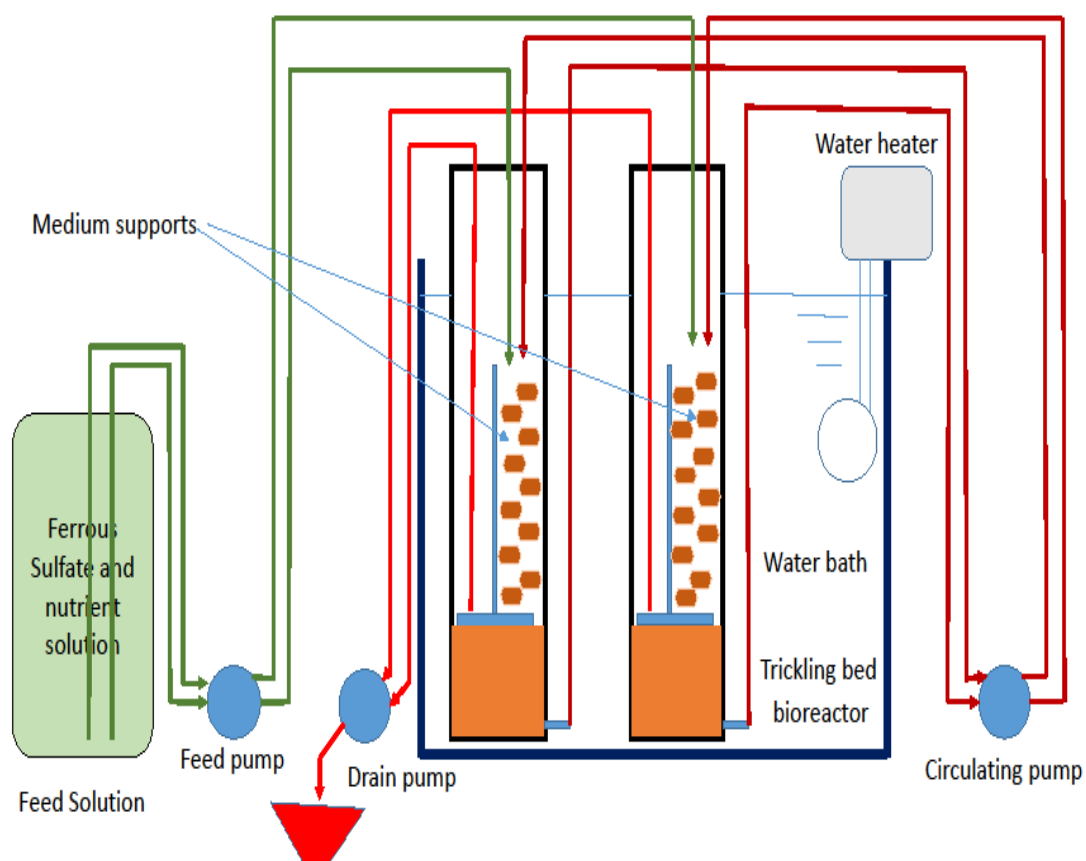


**Figure 15. Experimental setup of the trickling bed bioreactor.**



Both bioreactors were immersed in water bath with dimensions 60L x 42H x 32W cm. A thermostatic water heater (VWR, model 1112A) was used to maintain the temperature in the water bath at 40 °C, which is optimal for the microbial culture [2].

### 3.2.2 Microbial Culture and Liquid Medium

The microbial culture used in this study was obtained by mixing samples of acid mine drainage from four different sites: Iron Mountain (Richmond Mine), California, USA; Rio Tinto, Spain; copper mines near Kalugerovo, Bulgaria; and Pyhäsalmi Mine, Pyhäjärvi, Finland. The mixed sample was introduced to the 1.4L airlift bioreactor (described below) containing 9K medium, which was operated as a chemostat at gradually decreasing pH, starting from 2.0 and finishing at 0.6 within a period of four months [3]. The final microbial culture is dominated by *L. ferrooxidans* with a minor presence of the archae *Ferroplasma* and the red alga *Cyanidium caldarum* [4].

The liquid solution used for the growth of the microbial culture, was a modified 9K mineral medium [5] containing (per liter demineralized water): FeSO<sub>4</sub>·7H<sub>2</sub>O (234 g) containing 47 g Fe<sup>2+</sup>, (NH<sub>4</sub>) SO<sub>4</sub> (2 g), K<sub>2</sub>HPO<sub>4</sub> (0.5 g), MgSO<sub>4</sub>·7H<sub>2</sub>O (0.5 g) and KCl (0.1 g). The medium was adjusted to pH of 0.85 – 0.9 by adding concentrated H<sub>2</sub>SO<sub>4</sub>.

### 3.2.3 Biofilm Support Particles

The support particles were 2” polypropylene glass-filled Jaeger Tri-Packs (Raschig Jaeger Technologies, Ludwigshafen, Germany) spheres having a geometric surface area of  $280 \text{ m}^2 / \text{m}^3$ , 90% void space and a bulk density of  $99 \text{ kg} / \text{m}^3$ .

### 3.2.4 Analytical Procedure

The concentrations of  $\text{Fe}^{2+}$  and  $\text{Fe}^{3+}$  ions were measured according to a spectrophotometric method with sulphosalicylic acid as an indicator [6] using Cary 50 UV-visible spectrometer (Varian, Sydney, Australia). The ferrous iron concentration was determined by titration with 0.1 N potassium dichromate, using N-phenylanthranilic acid as an indicator [3].

## 3.3 Results and Discussion

Since one of the main goals of this study is determination of the effect of substrate feed interruption on the biochemical iron oxidation rate, the determination of the bioreaction rate will be discussed below.

The change in limiting substrate ( $\text{Fe}^{2+}$  in our case) concentration in a continuous bioreactor can be described by the material balance of the bioreactor, given as:

$$V_r \frac{dS}{dt} = FS_{in} - FS_{out} - V_r r_s \quad (3.1)$$

Where  $V_r$  is the liquid volume in the bioreactor,  $S$  is the substrate ( $\text{Fe}^{2+}$ ) concentration,  $F$  is the liquid flow rate,  $S_{in}$  and  $S_{out}$  are the inlet and outlet substrate concentrations and  $t$  is time. The rate of substrate consumption  $r_s$  can be given as [7]:

$$r_s = \frac{\mu_m X}{Y} \frac{S}{K_s + S} \quad (3.2)$$

Where  $\mu_m$  is the maximum specific growth rate,  $X$  is the microbial concentration,  $Y$  is the substrate/biomass yield coefficient and  $K_s$  is the Michaelis constant.

It has been shown that for the microbial culture used  $K_s=0.0067$  g/L [8]. Since in a trickling filter the amount of microorganisms remains constant within a day, for the case of  $S \gg K_s$  (i.e. approximately  $S > 0.1$  g/L) one can write Eq. 3.2 as:

$$r_s = \frac{\mu_m X}{Y} = \text{const} \quad (3.3)$$

When the substrate feed is stopped ( $F=0$ ), Eq. 3.1 becomes:

$$r_s = -\frac{dS}{dt} \quad (3.4)$$

I.e. the slope of the curve is constant, equal to the negative rate of biochemical reaction.

When, the feed is restarted again, the entire Eq. 3.1 is valid, and can be rewritten as:

$$r_s = \frac{F}{V_r}(S_{in} - S_{out}) - \frac{dS}{dt} \quad (3.5)$$

During steady-state bioreactor operation,  $dS/dt = 0$ , and Equation 3.1 becomes:

$$r_s = \frac{F}{V_r}(S_{in} - S_{out}) \quad (3.6)$$

Equations 3.4 and 3.5 were used to calculate the rate of biochemical reaction during the stopping of substrate feed, and during restarting it, respectively. Under steady-state conditions, Eq. 3.6 was used to calculate the rate of the ferrous iron biooxidation.

Figure 16 shows graphically the theoretical profiles of the substrate (S) concentration in time before, during and after stopping the feed flow rate (F) for a period  $t_s$ . The applicability of the above equations is shown also in Fig. 16. The figure also shows the curves when the feed interruption affects the reaction rate temporarily (line 2), permanently (line 1) or not at all (line 3). If during the period of feed stoppage ( $t_s$ ) the substrate is consumed completely (S reaches zero), there will be a period of no substrate in the liquid medium during the time  $t_o$  (Fig. 16). In the case of temporary effect of the feed interruption on the rate of iron biooxidation, the main parameters are the height of the substrate “bump” ( $S_h$ ) and the time to reach steady-state ( $t_h$ ).

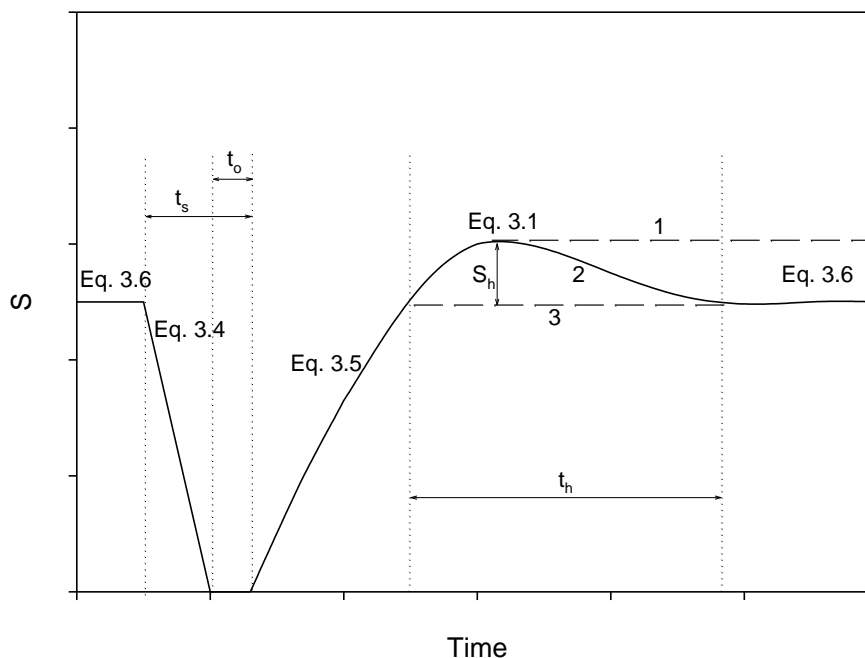


**Figure 16. Theoretical change of the substrate (ferrous ion) concentration in time during and after a feed flow interruption.**

The experiment was started by forming a biofilm on the support particles. The bioreactors were initially filled with cultural medium, thus submerging the support particles in it. The latter were occupying one of the two vertical sections of each bioreactor, while the second vertical section was aerated. Therefore, each bioreactor was acting as an airlift one. When a steady-state oxidation of ferrous iron was reported, the liquid was drained from the bioreactors (with the exception of the last 410 mL, as mentioned in the Materials and Methods) and they were converted to a trickling mode of operation. As soon as steady-state conditions were reached in both bioreactors under trickling mode, the experiments on the dynamics of the process were conducted. Under steady-state

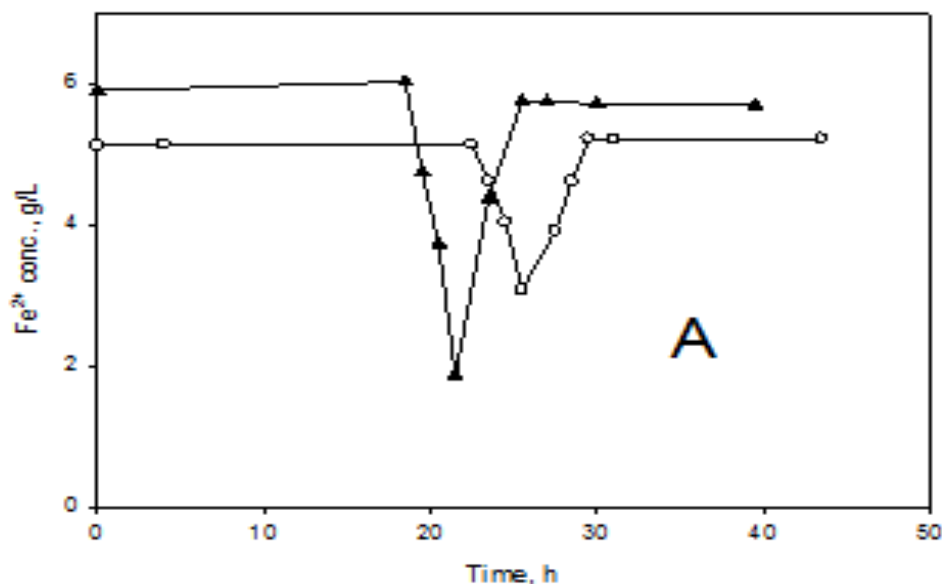
operation the input ferrous iron concentration was 47-50 g/L, and the ferrous iron oxidation was 85-90%.

The dynamics of the process of biological ferrous iron oxidation was studied by stopping the substrate feed to the bioreactors for different time periods, followed by restarting the feed at the original flow rate. The rates of the biochemical reaction before and after stopping the feed (under both steady-state and non-steady-state conditions) were determined.

The feed stoppage periods were: 3, 6, 16, 24, and 72 hours. These stoppage periods were selected to cover wide range of time the BioGenerator might be in standby operation due to the variations in operation of the renewable sources of energy (i.e. wind turbines or photovoltaics).

The experiment was run with both bioreactors as a duplicate. Both bioreactors showed the same trend with similar results.

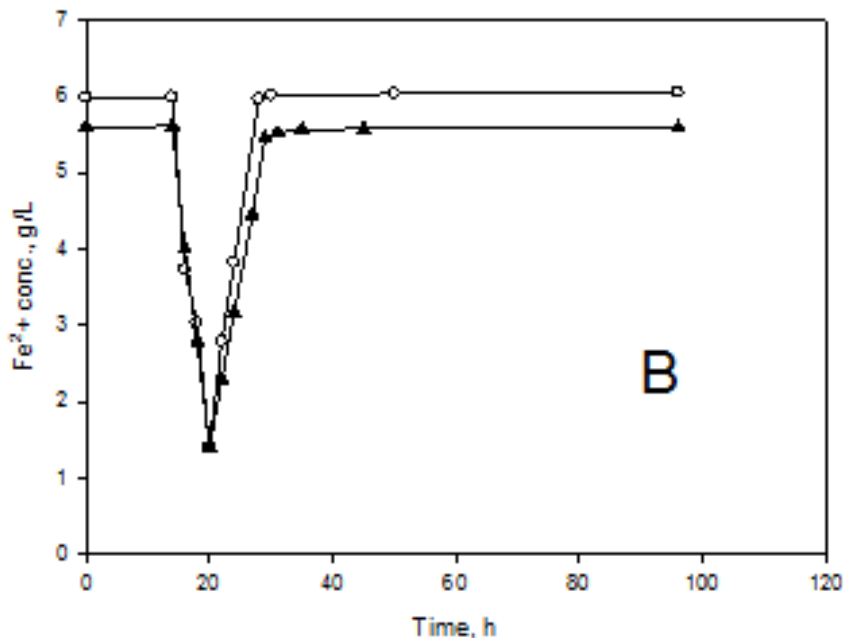
Figure 17 shows the profiles of ferrous iron concentration in time for bioreactor 1 and 2 at a feed stoppage interval of three hours. It can be seen that after the feed flow interruption, the iron biooxidation returned to its initial steady-state conditions. No temporary or permanent effect of the feed flow interruption on the rate of iron biooxidation was detected (both  $S_h$  and  $t_h$  were equal to zero).



**Figure 17. Experimental S-t curves for three hours feed flow interruption.**

The decline line in both curves indicates the oxidation of the microbial culture of the remaining ferrous in the bioreactor immediately after the feed flow stoppage. It is noticeable that the ferrous iron concentration dropped linearly from 5 to 3 g/L in the first bioreactor and from 5.9 to 2 g/L in the second bioreactor during the 3 hours feed flow stoppage. It is clearly noticeable that after restarting the feed flow (the ascending parts of the curves), the system needed another 3 hours to return completely to the previous steady state of ferrous oxidation rate.

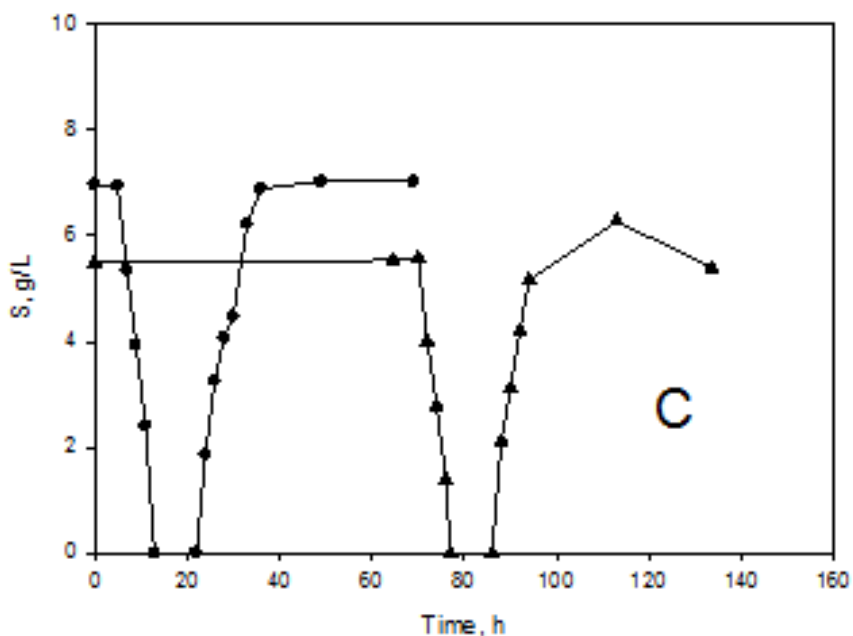
Figure 18 shows the results of the feed interruption for a period of six hours. The same trend can be observed as in the case of 3 hours feed flow interruption. The ferrous concentration dropped from about 6 g/L to less than 1 g/L after 6 hours feed flow stoppage and it took both bioreactors about 6 hours to return to the steady state oxidation rate after restarting the feed flow.



**Figure 18. The change of ferrous iron concentration in time for a 6 hours feed flow interruption.**

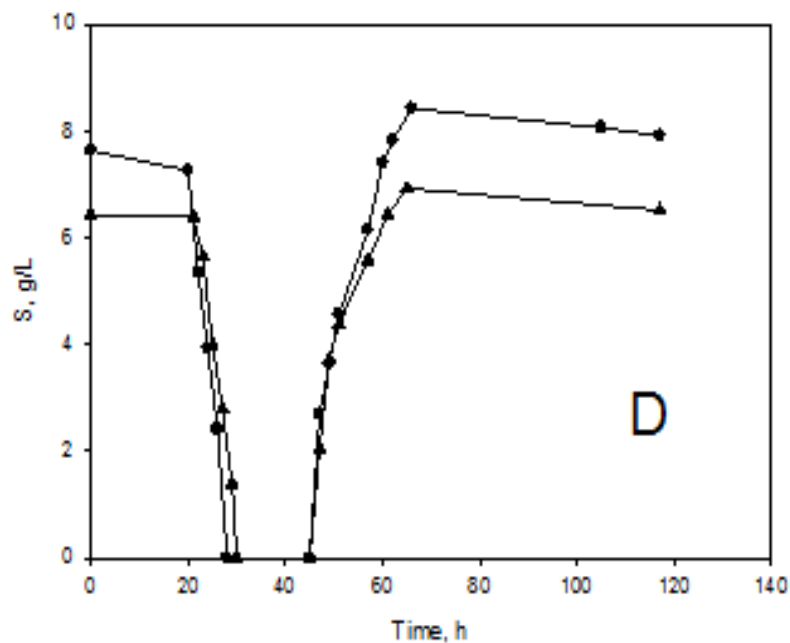
The results of feed interruption for a period of 16 hours are shown in Figure 19. It can be seen that it took the microbial culture 7 to 8 hours to consume all existing ferrous iron in both bioreactors after the feed flow was stopped. However, it took both systems around 14 to 20 hours to recover the depleted ferrous iron and return to the previous steady state ferrous oxidation rate. That is qualitatively expected, taking into account Eqs. 3.4 and 3.5, describing these two parts of the curve. Here both bioreactors showed slightly different results. While bioreactor 1 showed no “bump” in the substrate concentration curve, i.e. there was no effect of the flow feed interruption on the iron biooxidation rate, bioreactor 2 showed a small “bump”. It seems that the time interruption of 16 hours is on the boundary where the time period  $t_h$  changed from zero to a positive value.





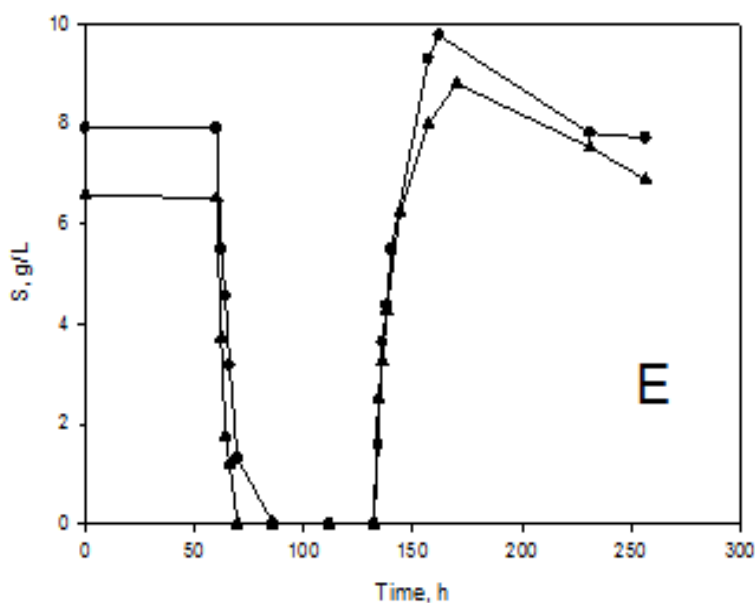
**Figure 19. Effect of the 16 hours flow interruption on ferrous iron concentration.**

In the next experiment, the feed to both bioreactors was stopped for a period of 24 hours (Fig. 20). It took the microbial culture 7 to 9 hours to oxidize all remaining ferrous in both bioreactors. The cultivating liquid remained with no ferrous iron (limiting substrate) for the rest of the 24 hours feed interruption period (i.e.  $t_h$  of 15 to 17 hours). The ferrous iron oxidation rate in the first 7 to 9 hours was  $0.82 \text{ g / (L.h)}$  while it was zero at the remaining 15 to 17 hours. It is expected that the microbial culture would be negatively affected by the lack of ferrous iron for the period of 15 to 17 hours. From both curves in figure 7, it can be seen that both bioreactors needed around 70 hours from restating the feed to reach their pre-disruption steady state oxidation rate. The brief “bump” in the ferrous iron concentration before reaching a steady-state value shows that there was a temporary decrease in the microbial activity after the flow interruption.



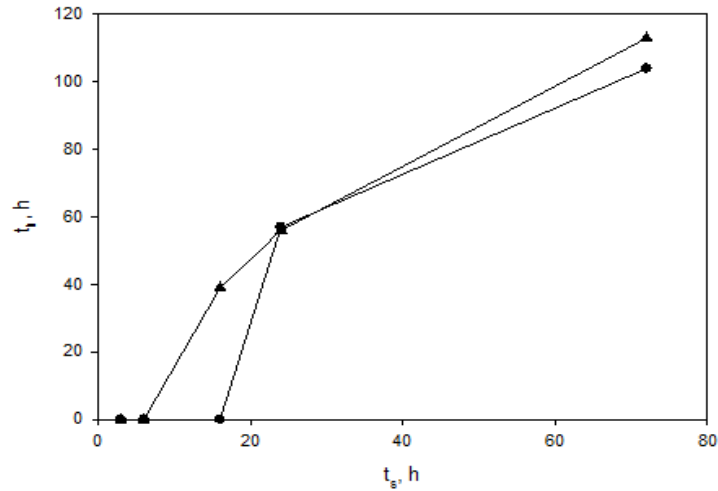
**Figure 20. Effect of the 24 hours flow interruption on ferrous iron concentration.**

Figure 21 shows the result of the 3 days interruption of the feed to both bioreactors. The oxidation rate in the first 9 to 10 hours was 0.65 and 0.7 g / (L.h) and zero g / (L.h) for the remaining 62 hours of feed stoppage. After restarting the feed, the increase of the substrate concentration was non-linear, as expected from Eq. 3.5. The “bump” in the substrate concentration curve was significantly higher ( $S_h$ ) and longer ( $t_h$ ) than in the case of one day flow disruption, which means that the microbial culture is affected stronger by the longer flow feed disruption and the longer period of zero ferrous iron concentration. It took both bioreactors around 100 hours for ferrous oxidation rate to return to the pre-interruption steady state rate.



**Figure 21. Effect of the 72 hours flow interruption on substrate concentration.**

Figures 17-21 show that the feed interruption has either no effect on the iron biooxidation rate (Figs. 17-18), or that the effect is temporary (Figs. 19-21). There are two main factors that would affect the iron-oxidation activity of microorganisms due to the interruption of the feed flow. First is the time length of flow interruption, and the second is the length of the period with zero or close to zero ferrous iron concentration  $t_o$  (Fig. 16). In this work the reduction of the microbial activity was described by two parameters: the maximum decrease in the iron biooxidation rate, corresponding to the height of the “bump” in the S-t curve ( $S_h$  in Fig. 16), and by the time required to reach the pre-disruption biooxidation rate ( $t_h$  in Fig. 16). Figure 22 shows the effect of the time of feed interruption  $t_s$  on the parameter  $t_h$ . It can be seen that the effect of the flow interruption on the rate of iron biooxidation starts at approximately  $t_s$  of 10 and 16 hours for bioreactor 1 and 2, respectively.



**Figure 22.** The relationship between the parameters  $t_h$  and  $t_s$ , as described in Fig. 15.

The effect of feed interruption time on  $S_h$  is shown in Fig. 23. The effect is roughly linear between interruption times of 10 and 72 hours. It should be noted that the reduction in the ferrous iron biooxidation rate appears when the ferrous iron concentration reaches zero during the feed flow disruption, i.e. at disruption times of 16 hours and more.

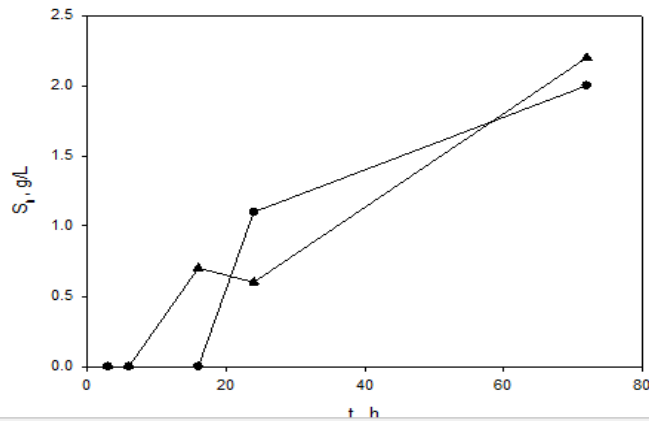


**Figure 23.** The relationship between the parameters  $S_h$  and  $t_s$ , as described in Fig. 16.

The reduction in the biooxidation rate due to the feed flow interruption is shown in Figure 24. It can be seen that while there is some rate reduction at interruption times above 16 hours, the rate reduction does not exceed 6%.

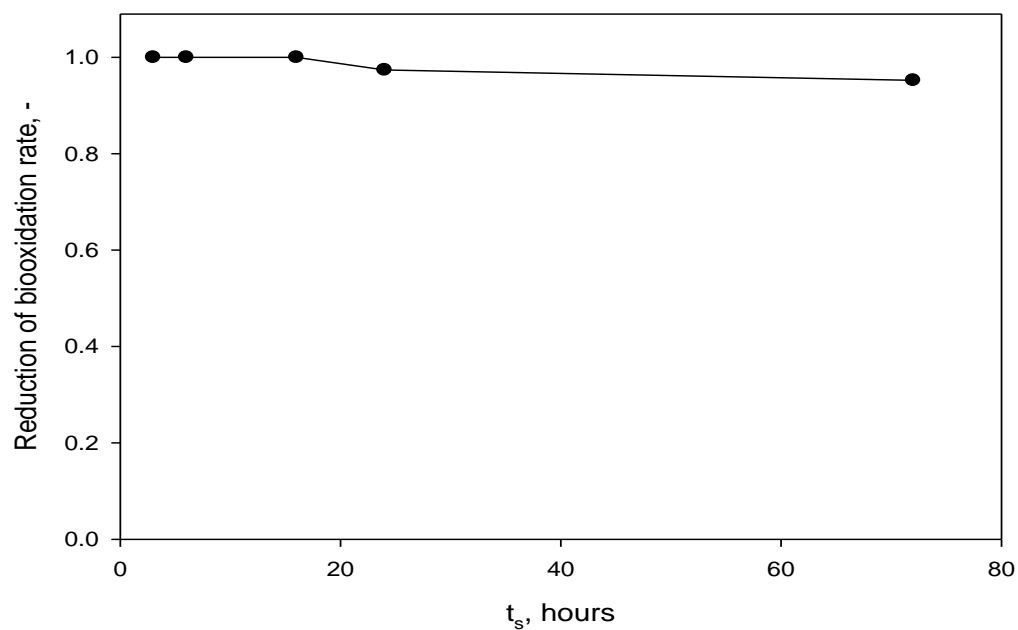


**Figure 24. The effect of the parameter  $t_s$  on the reduction of the ferrous iron biooxidation rate.**

### 3.4 Conclusions

This study shows the results of the dynamic behavior of the biooxidation of ferrous iron by *L. ferriphilum* in a trickling bed bioreactor. The process parameters were varied in order to assess the behavior of the bioreactor when used as part of the hydrogen-based energy storage system and smoothing of renewable power generation. The dynamics of the process was assessed by stopping the ferrous iron feed to the bioreactor during different time periods, varying between 3 and 72 hours. The feed stopping corresponds to the periods of maximum renewable power (wind or solar) generation. Our results show that if during the feed flow interruption, the concentration of ferrous iron in the bioreactor does not reach zero, there is no reduction in the iron biooxidation rate after resuming the feed flow. However, when the ferrous iron is completely consumed in the bioreactor during the feed flow interruption, there is a temporary decrease in the iron biooxidation rate after resuming the feed flow. The oxidation rate reduction in all cases was below 6%. These results show that the trickling filter bioreactor with *L. ferriphilum* is a promising system for use in a hydrogen-based energy storage system.

### 3.5 References

- [1] Karamanev, D. *Biofuel Cell*, US Patent #2006251959 (2003).
- [2] Penev, K. & Karamanev, D. Batch kinetics of ferrous iron oxidation by *Leptospirillum ferriphilum* at moderate to high total iron concentration. *Biochem. Eng. J.* **50**, 54-62 (2010).
- [3] Pupkevich, V., Scale-up and study of the BioGenerator, Ph.D. Thesis, The University of Western Ontario, 2014.
- [4] Penev, K., Kinetics of the ferrous iron biooxidation by *Leptospirillum ferriphilum* at high iron concentration, PhD Thesis, The University of Western Ontario, 2010.
- [5] Silverman, M. P., Lundgren, D. G. Studies on the chemoautotrophic iron bacterium *Ferrobacillus ferrooxidans*. I. An improved medium and a harvesting procedure for securing high cell yields. *J. Bacteriol.* **77**, 642-647 (1959).
- [6] Karamanev, D., Nikolov, L.N. & Mamatarikova, V. Rapid simultaneous quantitative determination of ferric and ferrous ions in drainage water and similar solutions. *Minerals Eng.* **15**, 341-346 (2002).
- [7] Shuler, M. L., Kargi, F. *Bioprocess Engineering*, Prentice Hall, 2001.
- [8] Penev, K., Karamanev, D., Batch kinetics of ferrous iron oxidation by *Leptospirillum ferriphilum* at moderate to high total iron concentration. *Biochem. Eng. J.* **50**, 54-62 (2010).

## Chapter 4

# 4 Cost Analysis of a 1 Megawatt Bio-Electrochemical Technology, The BioGenerator

### 4.1 Nomenclature

AOTR Actual oxygen transfer rate under field conditions, kg O<sub>2</sub> / h

$C$  Concentration (g / L)

$C_L$  Operating oxygen concentration, mg / L, in our case 2 mg / L

$C_{s,20}$  Dissolved oxygen saturation concentration in water at 20°C and 1 atm (mg / L)

$C_{sTH}$  Average dissolved oxygen saturation concentration in water in aeration tank at temperature T and altitude H (mg / L)

$C_{s,T,H}$  Oxygen saturation concentration in water at temperature T and altitude H (mg / L)

$D$  Diameter (mm)

$E$  Voltage (V)

$F$  Faraday's constant (C / Mole)

$g$  Gravity acceleration (m / s<sup>2</sup>)



$h$	Height (m)
$I$	Electrical current (A)
$k_L a$	Overall volumetric mass transfer coefficient (1/ h)
$O_t$	Percent oxygen concentration in air leaving the bioreactor, usually 18 to 20 %
$P$	Power (W)
$p$	Pressure (k Pa)
$P_d$	Pressure at the depth of air release (k Pa)
$P_{\text{atm,H}}$	Atmospheric pressure at altitude H (k Pa)
$P_{\text{w, mid depth}}$	Hydrostatic pressure at mid depth above the point of air release, due to water column (k Pa)
$Q$	Volumetric flow rate of liquid ( $\text{m}^3 / \text{s}$ )
SOTR	Standard oxygen transfer rate in clean water at 20 <sup>0</sup> C, and zero dissolved oxygen (kg O <sub>2</sub> / h)
$t$	Time (s)
T	Operating temperature (°C).

*Greek Letters*

$\alpha$  Oxygen transfer correction factor for water (-)

$\beta$  Salinity-surface tension correction factor (-)

F Fouling factor (-)

$\rho$  Density (kg / m)

*Subscripts*

$Fe^{2+}$  Relative to ferrous iron

$Fe^{3+}$  Relative to ferric iron

G Relative to gas

L Relative to liquid

$O_2$  Relative to oxygen

*Abbreviations*

GRP Glass reinforced plastic

PEM Proton exchange membrane

RCC Reinforced cement concrete

SS Stainless steel

USD US dollar

## 4.2 Introduction

The world is increasingly shifting from the use of fossil fuel-based power generation processes towards renewable primary energy sources. In addition to their obvious advantages, unfortunately wind and solar sources have a major drawback which requires comprehensive addressing prior to be used as a dependable standalone power generation source. The intermittent, unpredictable and variable rate of energy supply of both wind and solar makes them unreliable power generation sources. The availability and the variability of both sources on the minute, hour and day scales is a major problem. This problem can be best solved by using an integrated energy storage [1].

The gap between the power generation and consumption is not only a problem of wind and solar sources but it is also a major problem of other electricity power generation systems which occurs due to the variation of power consumption along the day and around the year [2].

Different energy storage systems have been proposed and employed. Among these, the hydrogen-based energy storage is considered to have a very good set of advantages [3].

The hydrogen based storage system contains three main components:

- Electrolyzer where excess electrical power is used to produce hydrogen gas by splitting water;
- Storage of the hydrogen produced by the electrolyzer;
- Re-electrification of hydrogen in a hydrogen to electricity convertor.

While the first two components of hydrogen energy storage (electrolysis and hydrogen storage) are relatively well developed, there is a lack of a commercial convertor of hydrogen to electricity. For a very long time it has been expected that fuel cells will be used for that. Unfortunately, some challenges in fuel cells development are still preventing their commercialization. As a result, there are still no profitable fuel cell companies world-wide [4]. These challenges include the high cost, the relatively low stability (short lifetime), and the lower than expected efficiency. The root of these challenges is analyzed below.

The major drawback of the PEM fuel cell is the extreme slowness reaction rate at the cathodic electrode of oxygen reduction [5]. As a result, the fuel cell is expensive (need of noble electrocatalyst), has a relatively short lifetime (because of platinum deactivation) and has a relatively low efficiency (because of the slowness of the reaction and the need for a high current density). These drawbacks have been encouraging many researchers to investigate many different mechanisms to accelerate reaction rates and to provide more commercially-viable technology solutions [6].

The BioGenerator is a bio-electrochemical system for electricity generation, which can overcome to a certain degree the main problems of conventional fuel cell.

#### 4.2.1 BioGenerator

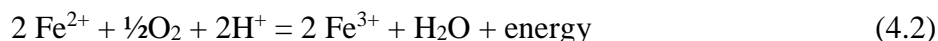
As stated earlier, one of the main problems of conventional fuel cells is the slowness of the oxygen reduction reaction (2.3). In nature the oxygen reduction reaction can be found mainly in the respiration chain of living aerobic organisms, such as animals

(including humans) and microorganisms. The first reaction in the respiration of these organisms is:



Obviously, the respiration reaction (4.1) looks exactly the same as the cathodic reaction in acidic  $\text{H}_2/\text{O}_2$  fuel cells (2.3). However, the rate of respiration within living organisms is by at least three orders of magnitude higher than the rate of the chemical reaction (2.3), even when using the most efficient electrocatalyst (i.e. platinum). Actually, the oxygen reduction reaction supplies electronegative energy to fuel cells as it is supplying electronegative energy to living organisms. In fuel cells the electronegative energy of oxygen is converted to electrical energy (plus waste heat), while in living organisms it is converted to mechanical, heat and chemical energy, needed by the organism to live.

In the BioGenerator [7], living microorganisms are used to convert the electronegativity of oxygen to electronegativity of ferric ions. The microorganisms used are *Leptospirillum ferriphilum*, which oxidize ferrous to ferric ions following the net reaction:



Equation (4.2) does not take into account biomass production which has a minor effect. Approximately 70% of the electronegative energy of oxygen is transferred to  $\text{Fe}^{3+}$ , while the rest is used by the microorganisms for their life. The produced ferric ions are then used as an electron acceptor in an electrochemical stack where they are reduced to  $\text{Fe}^{2+}$  and produce electricity. The cathodic ferric iron reduction (4.2) is by orders of magnitude faster than the electrochemical reduction of oxygen (2.3) and does not need an

electrocatalyst. Therefore, one very slow reaction (2.3) is replaced in the BioGenerator by two very fast reactions (4.1 and 4.2), requiring no noble electrocatalyst.

Therefore, the BioGenerator is a bio-electrochemical convertor of the energy of hydrogen oxidation (2.7) to electrical energy. It has significant higher electrical efficiency than conventional fuel cells, has potentially longer lifetime, and can be used for the hydrogen-based energy storage.

The BioGenerator has been extensively studied from the point of view of biokinetics [8], bioreactor design [9,10], electrode design [11], polymer membrane development [12,13], mathematical modelling [14]. It has been scaled up physically from the initial size of 0.1 Watt to 300 W [9]. Currently a pilot-scale 10 kW BioGenerator is being built as part of a wind and solar power management system. On the basis of these developments, we are currently able to propose a cost analysis of a large scale (1 MW) BioGenerator.

### 4.3 Purpose of This Study

In this study, 1 MW power generation capacity BioGenerator is theoretically scaled up and designed using an “airlift” bioreactor. Detailed cost analysis of the BioGenerator is performed.

## 4.4 BioGenerator Calculations

As stated earlier, the BioGenerator comprises of two main components; bioreactor and electrochemical stack.

### 4.4.1 Overall Calculations

In this study, the intended power generation of the BioGenerator is 1 MW, therefore:

$$P = V \cdot I = 10^6 \text{ W} \quad (4.3)$$

According to previous study [9], the optimal voltage (V) at the desired current density of 100 mA/cm is 0.7 V. Therefore, according to equation (4.3), the electrical current generated is  $1.43 \times 10^6$  A. The Faraday's constant F, equals to the electrical charge of one mole of electrons ( $M_{e^-}$ ), is 96500 C/Mol. Therefore, the formation or consumption of one  $M_{e^-}/s$  produces 96500 A. Since one mole of ferric ions consumes one mole of electrons (eq. 2.5), and the mass of one mole of  $Fe^{3+}$  is 55.8 g, then  $55.8 \text{ g}_{Fe^{3+}}/s$  produces 96485 A of electrical current. Therefore, the relationship between the electrical current generated, the ferric iron solution flow rate (Q) and the iron concentrations can be given as:

$$I = FQ \frac{C_{Fe_{in}^{3+}}}{MW_{Fe^{3+}}} \times \frac{C_{Fe_{in}^{3+}} - C_{Fe_{out}^{3+}}}{C_{Fe_{in}^{3+}}} \quad (4.4)$$

The usual feed concentration of  $\text{Fe}^{3+}$  is 50 g/L, 30% of which is reduced to  $\text{Fe}^{2+}$  in the electrochemical stack [9]. Therefore, according to Eq. 4.4, to obtain  $1.43 \times 10^6 \text{ A}$  of current, the required catholyte flow rate is 55.1 L/s or 200  $\text{m}^3/\text{h}$ .

#### 4.4.2 Bioreactor Calculations

The bioreactor is the part of the BioGenerator where the iron bio-oxidation reaction takes place. The main microbial species in the bioreactor is *Leptospirillum ferriphilum*, which is a chemo-autotrophic iron oxidizing microorganism. It uses ferrous ions as an electron donor, oxygen as an electron acceptor and atmospheric carbon dioxide as a carbon source. The microorganisms produce ferric ions, microbial mass and water according to reaction equation (4.2). The ferric ions produced in the bioreactor are reduced in the electrochemical cells, serving as an electron acceptor (oxidant) in the electricity generation:



The liquid in the bioreactor is maintained at pH between 0.7 and 0.9 at a temperature of 40°C. The total iron concentration in the bioreactor feed is 50 g/L, distributed between ferric and ferrous state. Maintaining sterile conditions in the bioreactor was not needed as at the ultra-low pH of the liquid prevents the contamination by unwanted microorganisms.



In this study, we are choosing an airlift type of bioreactor, having a typical volumetric iron biooxidation rate of  $1.5 \text{ g Fe}^{3+} / (\text{L}\cdot\text{h})$ , [9].

#### 4.4.3 Bioreactor Volume

The input mass rate of ferrous iron equals  $Q \cdot C_{\text{Fe}^{2+}\text{in}}$ , and therefore, is equal to  $3.0 \times 10^6 \text{ g/h}$ . The concentration of ferrous iron entering the bioreactor is equal to that leaving the electrochemical stack.

The required bioreactor volume can be calculated by dividing the input mass rate of ferrous iron to the bioreactor by the ferrous iron oxidation rate in the bioreactor. Hence, the required volume of liquid in the bioreactor is  $3.0 \times 10^6 (\text{g/h}) / 1.50 (\text{g}_{\text{Fe}^{3+}}/\text{L}\cdot\text{h}) = 2.0 \times 10^6 \text{ L}$  or  $2000 \text{ m}^3$

#### 4.4.4 Oxygen Requirement

The stoichiometric relationship between the rate of oxidation of ferrous iron and the rate of consumption of oxygen is shown in Equation (4.2). It can be stoichiometrically calculated that  $1 \text{ g O}_2$  is required for the oxidation of  $6.975 \text{ g}$  of ferrous ions.

Knowing the  $\text{Fe}^{3+}$  consumption rate in the electrochemical cell ( $R_{\text{Fe}^{3+}}$ ), equal to  $Q(C_{\text{Fe}^{3+}\text{in}} - C_{\text{Fe}^{3+}\text{out}})$  therefore  $R_{\text{Fe}^{3+}} = 200 (\text{m}^3 / \text{h}) \times (50 - (50 \cdot 0.7)) (\text{kg}/\text{m}^3) = 3,000 \text{ kg}_{\text{Fe}^{3+}} / \text{h}$ .

Thus, the amount of oxygen required to oxidize the ferrous iron entering the bioreactor is  $3,000 / 6.975 = \text{AOTR} = 430 \text{ Kg}_{\text{O}_2} / \text{h}$ .

#### 4.4.5 Correction Factors for Oxygen Demand

The amount of air needed to supply the required oxygen to the bioreactor can be determined by taking into account factors affecting the gas-liquid oxygen transfer rate, such as salinity surface tension, temperature, elevation, diffused depth (for diffused aeration system), desired oxygen operating concentration, and the effects of mixing intensity and bioreactor configuration. The relationship between these factors is given by the following equation [15]:

$$AOTR = SOTR \left( \frac{\beta C_{s,T,H} - C_L}{C_{s,20}} \right) (1.024^{T-20})(\alpha)(F) \quad (4.6)$$

Where AOTR is the actual oxygen transfer rate under field conditions, kg O<sub>2</sub>/h; SOTR is the standard oxygen transfer rate in clean water at 20<sup>0</sup> C, and zero dissolved oxygen, kg O<sub>2</sub> /h,

$C_{s,T,H}$ , is the average dissolved oxygen saturation concentration in clean water in the bioreactor at temperature T and altitude H, mg / L.

$$C_{s,T,H} = C_{s,T,H} \frac{1}{2} \left( \frac{P_d}{P_{atm,H}} + \frac{O_2}{21} \right) \quad (4.7)$$

$$\alpha = \frac{K_L a (bioreactor liquid)}{K_L a (water)} \quad (4.8)$$

From table D-1 (Appendix D) [15]: C<sub>20</sub> = 9.08 mg /L and C<sub>40</sub> = 6.41 mg /L

Here we assume a sea level altitude, i.e.  $P_d/P_{atm,H}=1$ . Therefore, the oxygen saturation concentration in water at 40 °C and sea level is 6.41 mg /L, and the atmospheric pressure in meters of water at sea level is 10.33 m.

The average oxygen concentration inside the bioreactor, assuming the percentage of oxygen concentration leaving the bioreactor tank is 19% and the liquid depth inside the tank is 4.5 m and the diffusers height from the bottom of the tank is 0.5 m, can be determined by the following equation:

$$C_{\overline{s,T,H}} = (C_{s,T,H}) \left( \frac{1}{2} \right) \left( \frac{P_{atm,H} + \rho_w \cdot Eff \cdot Depth}{P_{atm,H}} + \frac{O_t}{21} \right) \quad (4.9)$$

Therefore,  $C_{\overline{s,T,H}} = 7.15 \text{ mg / L}$

To determine SOTR, a literature data of  $K_{L\alpha}$  in a liquid similar to that in the bioreactor was used [9] as well as in tap water [15]. These data showed a value of the parameter  $\alpha$  within the range between 1.85 and 2.7. In this study,  $\alpha$  value equals to 2.0 is used for further calculations. Also, salinity-surface tension correction factor  $\beta=0.95$ , fouling factor  $F=0.9$ , dissolved oxygen saturation concentration in clean water at 20 °C and 1 atm  $C_{s,20} = 9.08 \text{ mg / L}$ , and the required operating oxygen concentration  $C_L = 2 \text{ mg / L}$ , were all used in equation (4.6), where  $AOTR = 430 \text{ kg O}_2 / \text{h}$ .

SOTR was calculated =  $282 \text{ kg O}_2 / \text{h}$ .

Hence, the required air flow rate can be calculated as:

$$Q_{air} = \left[ \frac{SOTR}{(E)(\rho)} \right] \quad (4.10)$$

Where E is the oxygen transfer efficiency for the diffusers used to aerate clean water. The density of air  $\rho$  at 40 °C and pressure of 101.3 k Pa can be determined from the ideal gas law:

$$\rho_a = \frac{P M}{R T} \quad (4.11)$$

Where the mean molecular weight of air M is 28.97 kg / (kg\*Mole). The temperature T was assumed to be 313.15 °K. Therefore,  $\rho_a = 1.127 \text{ kg / m}^3$  and the partial density of oxygen in air is  $0.2615 \text{ kg}_{O_2} / \text{m}^3$ .

For immersed air dispersion, two main aerator types are available. The first type is fine bubble diffusers producing mostly spherical bubbles between 1 and 3 mm in diameter. These diffusers can be in the form of porous plates, discs or domes (ceramic or plastic), or perforated plastic or rubber membranes. The small bubbles have a high surface area per unit volume, provide good oxygen-liquid contact, leading to relatively high oxygen transfer efficiency. The main disadvantage of the small orifice diffusers is the high maintenance cost in some application owing to orifice clogging by microorganisms.

The second main type of aerators is coarse bubble diffusers, with orifices of 5 to 12 mm in diameter, producing large, non-spherical, rapidly rising bubbles that can be as large as 50 mm in diameter. The coarse bubble diffusers have lower oxygen transfer efficiency than fine bubble type, since the gas-liquid interfacial area for oxygen transfer is

considerably smaller. However, coarse bubble diffusers have the advantage of lower maintenance.

The fine bubble diffusers require less than half the aeration power per mass of oxygen transferred compared to coarse bubble diffusers and the choice between fine and coarse bubble diffusers often depends on the cost of the power versus the cost of the maintenance. The oxygen transfer efficiency depends on the bubble size and the air flow rate delivered per unit surface of the diffuser, which is specific to the type and configuration of the diffuser. Therefore, more accurate figures of the oxygen transfer efficiency and air flux range per unit diffuser need to be provided by the diffusers' suppliers.

In our case the aerated liquid is a strong oxidant with pH below 1 at temperature of 40 °C. Therefore, diffusers with suitable material of construction are very limited.

Unfortunately, the most popular ceramic fine bubble diffusers used in wastewater treatment cannot be used in the BioGenerator due to their low chemical stability. The popular Sanitaire polyurethane and EPDM fine bubble diffusers (Xylem Inc., Rye Brook, NY, USA) provide air flux in the range of 3.7-37 Nm<sup>3</sup> / (h.m<sup>2</sup>), have a standard oxygen transfer efficiency of 7-10% per meter of submergence and a standard aeration efficiency of 3-8 kg O<sub>2</sub> / kWh for Polyurethane fine bubble diffusers. In the case of EPDM fine bubble diffusers, at a flux range between 0.8 and 7 Nm<sup>3</sup> / h per disc, the standard oxygen transfer efficiency is 6.5% per meter submergence and the standard aeration efficiency (SAE) is between 2.5 and 6 kg O<sub>2</sub> / kWh. Another possible option from the same

manufacturer is a coarse bubble diffuser made from 304 and 316 stainless steel, having air flow rate between 15 and 63 Nm<sup>3</sup> / h, SOTR between 1.6 and 2.5% per m submergence, and SAE in the range of 0.7-2 kg O<sub>2</sub>/ kWh.

Based on the supplier's information, the required air flow was calculated for each option (i.e. fine and coarse bubble diffusers) below.

SOTR of a fine bubble diffuser is 30-45% with 4.0 m submergence, therefore, 40% is used in the calculations below. Also, SOTR of coarse bubble diffusers is 7.2-11.2% at 4 m submergence; 11% is used in the calculations below.

Therefore, the required air flow in case of fine bubble diffusers can be calculated as:

$$Qa = \left[ \frac{282 \text{ (Kg O}_2\text{/h)}}{(0.40)(60 \text{ min/hr})(0.2615 \text{ Kg O}_2\text{/m}^3 \text{ air)}} \right] = 45 \text{ m}^3 \text{ /min or } 2,700 \text{ m}^3 \text{ / h}$$

Therefore, the number of required diffusers in the case of 10 Nm<sup>3</sup> / h air flow rate per unit is 270.

The required air flow in the case of coarse bubble diffusers is:

$$Qa = \left[ \frac{282 \text{ (Kg O}_2\text{/hr)}}{(0.11)(60 \text{ min/hr})(0.2615 \text{ Kg O}_2\text{/m}^3 \text{ air)}} \right] = 163 \text{ m}^3 \text{ / min or } 9,800 \text{ m}^3 \text{ / h}$$

Therefore, in the case of 50 Nm<sup>3</sup>/h air flow rate per diffuser band, approximately 200 bands are required.

#### 4.4.6 Hydrogen Requirement

The stoichiometric relationship between the rate of iron biooxidation and the rate of hydrogen consumption is given by equation (4.2). Therefore, for 118 g  $\text{Fe}^{3+}$ , 2 g  $\text{H}^+$  are needed, equivalent to 1 g  $\text{H}_2$ .  $\text{Fe}^{3+}$  oxidation rate =  $Q (C_{\text{in}} - C_{\text{out}}) = 200 (\text{M}^3 / \text{h}) \times (50 - 50(0.7)) (\text{g} / \text{L}) = 3,000 \text{ kg} / \text{h}^1$

Therefore, the hydrogen demand is  $3,000/118 = 25.4 \text{ kg}_{\text{H}_2} / \text{h}$  or  $0.42 \text{ kg}_{\text{H}_2} / \text{min}$

### 4.5 Sizing of Equipment

#### 4.5.1 Sizing of the Bioreactor Tank and Other Civil Engineering and Construction Requirements

As previously calculated, the total required volume of the bioreactor is  $2000 \text{ m}^3$ . The selected liquid depth in the tank is 4.5 m as it is considered within the optimal range of depth for oxygen transfer when using air diffusing system. Also, 5 m wall height for the concrete tank is considered a good practical option for the easiness of erection and lower cost. The tank is divided into 10 compartments with dimensions of 10 m x 5 m x 5m, as shown in figure 25. This division would give the bioreactor the option to work below its full capacity and provide the possibility to isolate one or more compartments for maintenance purposes. In addition, having compartments with 5 m width will allow the

installation of vertical dividing walls if needed to provide an air lift mechanism for effective circulation inside the compartment and greater oxygen transfer rate.

Based on the required operational conditions (i.e. pH of 0.7-0.9 and temperature of 40°C), the available practical bioreactor tank material of construction options are very limited. The most appropriate materials of construction for the bioreactor tank can be either acid resistant-lined concrete or stainless steel 316L.

In our case we selected the bioreactor tank material of construction to be steel-reinforced concrete (RC) with acid resistant epoxy coating inside the tank and waterproof insulation outside the tank. The steel bars used will be epoxy coated for more effective corrosion protection in the case of any seepage of the bioreactor liquid solution through the concrete foundation or walls.

The tank can be built either underground level, which is preferable for more temperature control, or above ground level for easier accessibility to the equipment room, which has to be adjacent to the tank. Therefore, in the case of the underground level option, the plant room should be constructed underground level in order to get the benefit of the net positive suction head for the circulation pumps.

The concrete tank in our application has many advantages over the stainless steel tank option, such as; durability of the acid resistant epoxy coating, lower cost for larger size, and easier maintenance. However, a plastic/ fiber glass tank would be even more appropriate for our application against concrete and steel tanks with only limitation being the commercial availability of plastic tanks with the required size and configuration.



With proper maintenance, the life time of a RC tank can reach up to 50 years.

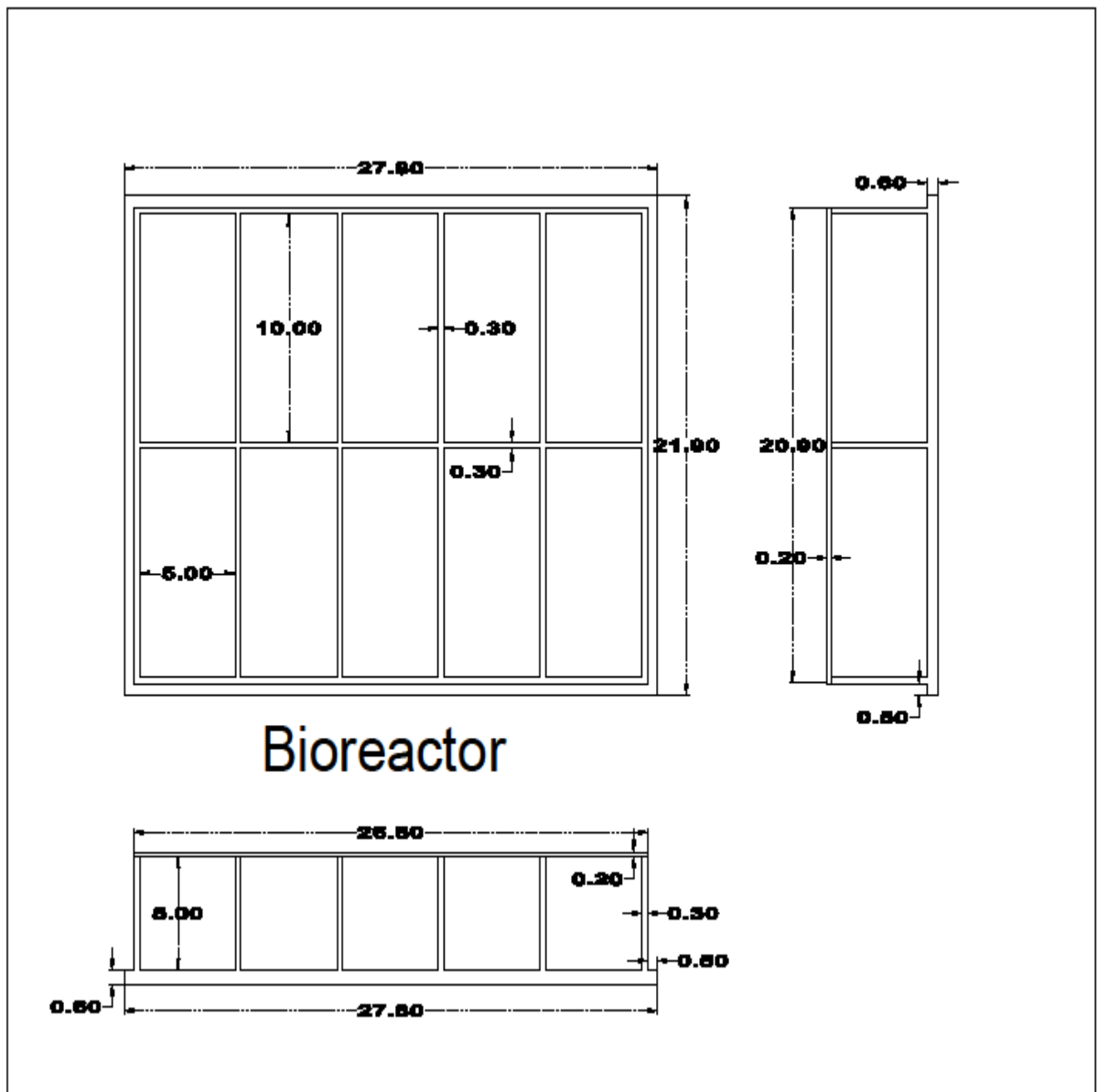


**Figure 25. Bioreactor concrete tank dimensional layout**

The above foundation, walls and roof thicknesses were selected on the basis of ordinary silty sand soil type with bearing capacity of  $1.5 \text{ kg / cm}^2$  or higher and 4.5 meter liquid depth inside the tank, and 4 meters under the ground level installation of the tank.

However, other technical details such as required steel reinforcement for the different parts of the tank, grade of the concrete and any required additives might be needed to enhance the strength and the curing of the concrete, are left for the structural engineering. The concrete wall thicknesses were selected based on previous application of similar tank sizes in wastewater treatment.

Therefore, the total RC volume for the bioreactor tank can be summarized as follows:

- 1- Foundation: 365.3 m<sup>3</sup> RC
- 2- Walls: 300.6 m<sup>3</sup> RC
- 3- Roof: 112 m<sup>3</sup> RC
- 4- Total RC amount: 778 m<sup>3</sup>

The total inner surface area of the tank to be covered with acid-resistant epoxy is 2,500 m<sup>2</sup> and the total outer surface area of the tank to be water proofed is 1195 m<sup>2</sup>. The total required excavation for the bioreactor tank and for the plant room is expected to be 5200 m<sup>3</sup>.

The design also includes underground plant room with dimensions of 20 x 15 x 5 m to contain the equipment (i.e. pumping stations, air blowers, electrochemical stacks, electrical and control panel, and an office room).

#### 4.5.2 Sizing of Circulating Pumps

From the above calculations, the required flow rate of liquid to be circulated between the bioreactor and the electrochemical stack is 200 m<sup>3</sup> / h. Since the ground area

of the bioreactor tank is quite large (27.8 m x 21.9 m), two sets of pumps are selected, as each set will serve half of the bioreactor tank (i.e. 5 compartments).

As mentioned above, the physical parameters of the circulating liquid between the bioreactor and the electrochemical stack are: pH 0.7-0.9, density 1200 kg / m<sup>3</sup>, temperature 40° C.

Thus, the required pumping sets are selected as follows:

Two sets of (3 duty / 1 standby) centrifugal end suction pumps, each pump has flow rate: 35 m<sup>3</sup> / h , and 3 bar head complete with gate valve on the suction side and both gate and non-return valves on the discharge side.

The material of construction of the pumps is either SS316L or a plastic which can handle the bioreactor liquid. The electrical motor of the pump: 10 kW, 380 V/ 3 ph / 60 Hz.

### 4.5.3 Sizing of Air Blowers

From the previous calculations, the required air flow rate in the case of fine bubble diffusers is 45 m<sup>3</sup> / min, and in the case of coarse bubble diffusers is 163 m<sup>3</sup> / min.

However, for the fine bubble diffusers option, the following is selected:

Two sets of (2 duty / 1 standby) Rotary Lobe Air Blowers, with individual flow rate of 810 m<sup>3</sup> / h, head 800 mbar, motor: 30 kW / 380 V / 3ph / 60 Hz.

From the previous calculation the required fine bubble diffusers are 270 units will be distributed equally and homogenously in all the ten compartments. The distance between

each two diffusers should be equal at both length and width directions in order to assure well distributed oxygen supply and proper mixing all over the compartments.

However, for the coarse bubble diffusers option, the following is selected:

Two sets of (4 duty / 1 standby) Rotary Lobe Air Blowers, with individual flow rate of 1340 m<sup>3</sup> / h, head 800 mbar, motor: 45 kW / 380 V / 3ph / 60 Hz.

According to the above calculations, the required number of coarse bubble diffuser bands is 200 units, and the same above arrangement in the case of fine bubble diffusers will be considered with the coarse bubble diffusers.

A hydraulic head of 800 mbar is selected for all air blowers to cover the pressure losses inside the air delivery pipes and fittings and also to overcome the 4 meters liquid depth in the bioreactors.

The power consumption by air blowers in case of coarse bubble diffusers is 360 kW, which is three times higher than that for fine bubble diffusers 120 kW. Therefore, fine bubble diffusers option is selected in our design.

#### 4.5.4 Sizing of Liquid and Air Pipelines

##### 4.5.4.1 Sizing of Liquid Pipeline

The material of construction for the liquid pipelines and valves should be suitable to handle liquid with low pH and temperature of 40°C. Stainless steel 316L piping is

considered an appropriate choice for its higher durability of the liquid condition. While SS 316L is relatively expensive, it is probably the most appropriate material.

At each side of the bioreactor, a suction puddle piece made of SS 316L will be installed 0.5 meter above the bottom of each compartment. Those five suction puddle pieces will be connected to a single suction pipeline delivering liquid from the five bioreactor compartments to the pumping station.

In order to maintain the velocity of the liquid inside the suction pipeline below 1 m / s, the main suction pipeline of each of the pumping stations should have a diameter of 200 mm. The approximate pipe length is 35 m. Each suction puddle piece has a diameter of 100 mm and 1 meter long.

The liquid velocity inside the discharge pipeline should be maintained below 2 m / s, and therefore the main discharge pipe for each of the two pumping stations needs to have a diameter of 150 mm. The main discharge pipeline will deliver the liquid to the electrochemical units via smaller branches. All pipes and fittings shall be of Schedule 40, SS 316L.

Two local SS 316 gate valves will be installed, one on the suction branch and the other on the discharge branch of each bioreactor compartments. Also, one SS 316 gate valve will be installed on the main suction pipeline. A non-return valve on the discharge pipeline of each pumping station will be installed as well.

#### 4.5.4.2 Sizing of Air Pipeline

All air blowers in each of the two sets will be connected to one main discharge pipeline made of black steel and the submerged branches made of SS 316L.

Both air blower sets will be located inside the plant room near to air inlet openings. Each air blowers set will run one main discharge pipeline on the top of the bioreactor and down-comer brunches will run inside the tank holding the air diffusers in the bottom of each compartment. As mentioned earlier, the total required number of air diffusers in case of fine bubble aeration is 270 which means 27 diffusers in each compartment. Each compartment will have 9 aeration branches with 3 diffusers on each branch.

Each air blower set will supply  $1,350 \text{ m}^3 / \text{h}$ . The air velocity inside the main air discharge pipe will be maintained around  $25 \text{ m} / \text{s}$ , therefore, the main air discharge pipe diameter will be 200 mm and its length is 35 m and will be of black steel pipe schedule 40. For each compartment, SS 316L branch pipe will run from the main air pipeline on the top of the bioreactor down to the bottom of the compartment. Many branches will run in the bottom of the compartment to hold the required air diffusers in even distribution. The SS 316L pipe branches will be of 50 mm diameter and each compartment branch should have a gate valve on the top of the branch. Figure 26 illustrates the whole plant (BioGenerator) layout and process flow diagram.

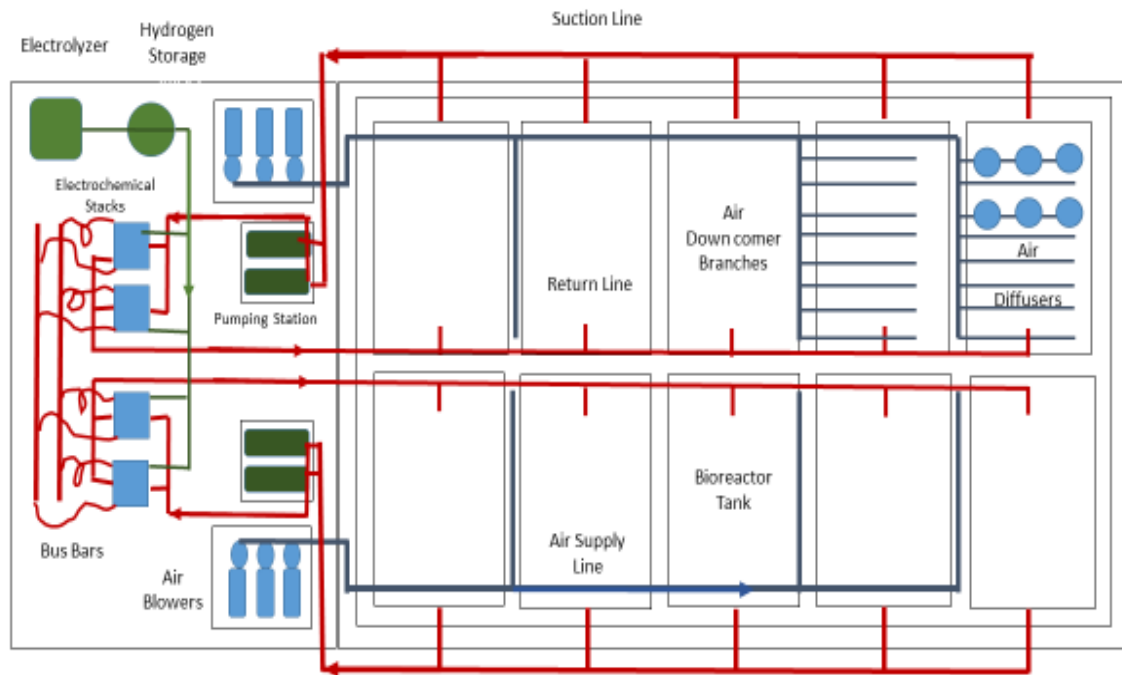


**Figure 26. Plant layout and the process flow diagram of the BioGenerator.**

#### 4.5.5 Electrical Supply

A power source is needed to supply the whole plant with electricity to enable the BioGenerator to produce 1 MW electricity. The total required power is 180 kW, 380 V/ 3 ph / 60 Hz in case of fine bubble diffusers option.

#### 4.5.6 Mist Eliminator

An individual mist eliminator unit will be installed on the top of each compartment. The function of these mist eliminators is to remove the acidic liquid mist

from the exhaust air of each compartment and return it back to the bioreactor. The mist eliminator can be of a fiber glass vessel containing packing plastic material, suction fan at the top of the vessel, and clean water shower at the top of the vessel. The suction fan will suck the air from the top of the bioreactor compartment through air duct connected to the mist eliminator. The air that carries acidic liquid mist will pass through the packing material and the water shower will return the acidic liquid back to the bioreactor. Only air free of mist will pass out of the mist eliminator.

#### 4.5.7 Water Heater and Temperature Control

As mentioned above, the liquid temperature in the bioreactor needs to be maintained at 40°C. This temperature is considered to be within the optimum temperature range for the growth of *Leptospirillum ferriphilum* microorganisms [8].

The energy released by the overall electro-bio-chemical reaction in the BioGenerator, equation (4.2), equals to 142 MJ / kg<sub>H<sub>2</sub></sub>, is distributed between electrical energy (product) and heat loss. At an electrical efficiency of 70%, the amount of heat released to the liquid medium in the BioGenerator is 42 MJ / kg<sub>H<sub>2</sub></sub>. At the same time, the main heat losses in the BioGenerator are due to the latent heat of water evaporation during the aeration of the bioreactor, and due to the heat transfer through the bioreactor walls to the surroundings. Therefore, in order to decrease the heat losses and maintain a temperature of the bioreactor liquid at 40°C, thermal insulation surrounding the bioreactor need to be provided. A further detailed analysis of the bioreactor heat balance should be conducted based on the climate profile at the intended location.



#### 4.5.8 Electrochemical Cell Stacks

In addition to the bioreactor, the electrochemical cell stack is the second main component of the BioGenerator. A schematic view of the electrochemical stack used in the BioGenerator is shown in Figure 27. The main elements of the stack include: anode, cathode, proton conductive membrane, bipolar plates, current collector plates and end plates. Except for the type of cathode and the membrane, almost all other elements of the stack are similar to those of a polymer electrolyte membrane (PEM) fuel cell. The cathode in the BioGenerator stack is an activated carbon felt type [11], while the membrane can be an inert, non-ion exchange, polyvinyl alcohol film [12].

The desirable current density in the electrochemical stack is  $100 \text{ mA} / \text{cm}^2$  which is equivalent to  $1000 \text{ A} / \text{m}^2$  of electrode surface. Therefore, the power produced by  $1 \text{ m}^2$  of electrode surface in the electrochemical cell is  $1000 \text{ A} \times 0.7 \text{ V} = 700 \text{ W}$ , or  $0.7 \text{ kW}$ .

Therefore, in order to produce  $1 \text{ MW}$  electricity, the total electrode surface equals to:  
 $1000 \text{ kW} / (0.7 \text{ kW} / \text{m}^2) = 1,430 \text{ m}^2$ .

Assume using surface area of a single electrochemical cell of  $20 \times 20 \text{ cm}^2$ , which means for  $1 \text{ MW}$  BioGenerator,  $35,750$  single cells are needed.

Alternatively, if the surface area of a unit cell of the electrochemical stack has the size of  $1 \times 1 \text{ m}^2$ , the BioGenerator needs  $1,430$  units and each unit has one anode, one cathode, one membrane and two bipolar plates.

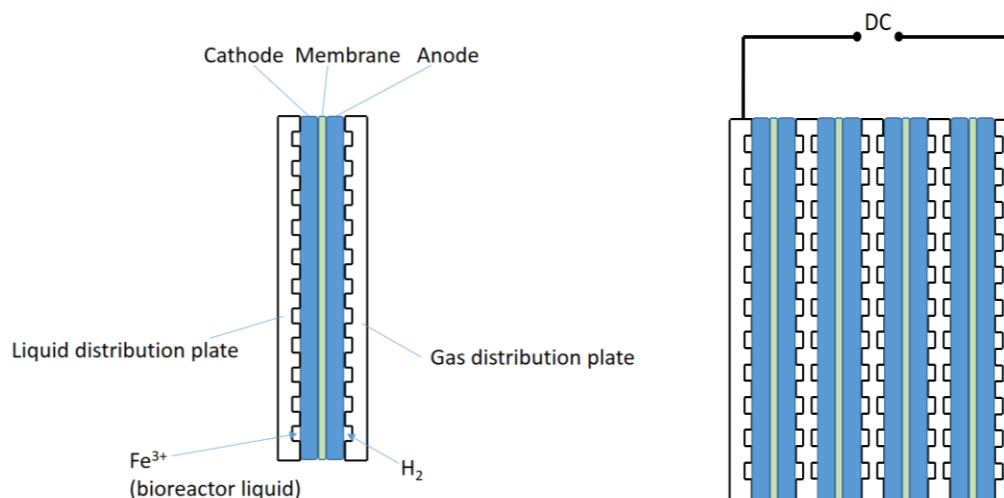


**Figure 27. Schematic view of the electrochemical stack used in the BioGenerator**

## 4.6 Cost Calculations

In this study all cost calculations were based on budgetary prices, Canadian local market prices, valid website price-lists, and other were estimated based on updated prices. All costs are given in US dollars for easier evaluation and comparison.

### 4.6.1 Civil and Construction Work

This scope of work includes all civil and construction work; mainly site preparation, soil testing, excavation, compaction, backfilling, structural design, RC construction of the bioreactor tank, RC construction of the plant room, water proofing for

the external walls of the tank, acid resistant treatment for internal surfaces of the tank, concrete testing and cracks repairing, manholes, and paddle pieces.

As the bioreactor RC tank will be constructed under the ground level, the outer surface of the tank's foundation and walls have to be water proofed with double layers of bituminous membrane to prevent water seepage from the surrounding soil to the inside of the tank.

The total RC tank and plant room construction cost was estimated by multiplying the total RC volume (previously calculated in section 5.1) by the concrete unit price per m<sup>3</sup> which includes labor, material, formwork and workmanship costs.

The cost of soil excavation, inner surface application and outer surface water proofing were also determined by multiplying their quantities times their estimated unit cost of each item. Table 2 shows the scope of civil work, the estimated unit price and the total cost of the work.

**Table 2. Civil scope of work for the bioreactor tank and the plant room, estimated unit prices and the total cost of the work.**

Item no.	Work description	Quantity  Volume or area	Unit	Unit Price  USD	Total Price  USD
----------	------------------	-----------------------------------	------	-----------------------	------------------------

1	Soil excavation for both tank and plant room, 45 X 24 X 5 m	5,400	M <sup>3</sup>	20.0	108,000
2	Backfilling around the tank and the plant room; approximately 1000 m <sup>3</sup>	1,000	M <sup>3</sup>	20.0	20,000
3	RC tank construction	778	M <sup>3</sup>	1,500	1,167,000
4	Plant room RC construction	360	M <sup>3</sup>	1,500	540,000
5	Inner surfaces acid-resistant coating	2,500	M <sup>2</sup>	50.0	125,000
6	Outer surfaces bituminous water proofing	1,600	M <sup>2</sup>	50.0	80,000
7	Puddle pieces, 316 SS, 4 in, Sch. 40	10	Each	1,000	10,000
8	Manhole and tank inside ladder	10	Each	2,000	20,000
	Total Price				2,070,000

### 4.6.2 Circulating Pumps

There are a large number of pumps' models that are suitable for our application. However, stainless steel 316 was selected as the material of construction of the pumps.

### 4.6.3 Air Blowers

Two separate air blower sets, each set have 2 duty / 1 standby air blowers were selected to serve the bioreactor. Each air blower set includes main discharge pipeline connected to 45 branches, 9 branches for each tank compartment. Each branch has a gate valve for possible disconnection from the main pipeline.

The selected air blower is of a "Rotary Lobe" type, it is used with many different applications and its capacity is considered of the low range capacity. This air blower type is supplied by many different manufacturers. However, the used price is an update of old price-list and considered of the high range of prices.

### 4.6.4 Air and Liquid Piping

This scope includes all required pipes and fittings for all components of the BioGenerator. The piping contains the main discharge and branches pipelines of the air blower sets, and the suction and discharge pipelines of the circulating pumping sets.

Table 3 summarizes the quantities, sizes, type of material, unit price, and the total price.

**Table 3. Pipeline quantities, their estimated unit prices and the total price.**

Item no.	Pipeline description	Quantity, m	Unit Price, USD	Total Price, USD
1	Air blower main discharge pipeline, galvanized steel schedule 40, 8 inch diameter	80	50	4,000
2	Air blower branches pipeline, galvanized steel schedule 40, 4 inch diameter	60	25	1,500
3	Air blower branches pipeline, stainless steel 316, schedule 40, 2 inch diameter	900	45	40,500
4	Pumping station main suction pipeline, stainless steel 316, schedule 40, 8 inch diameter	70	300	21,000
5	Pumping station main discharge pipeline, stainless steel 316, schedule 40, 6 inch diameter	70	200	14,000
6	Electrochemical stack units in and out	200	45	9,000

	pipeline connections, stainless steel 316, schedule 40, 1 inch diameter			
7	Miscellaneous	1	Lot	70,000
	Total amount for pipes and fittings			160,000

The total price includes material cost, delivery and site installation. However, used prices are valid prices at suppliers' websites.

#### 4.6.5 Electrical and Control

The quoted price for this item was estimated to cover for all electrical and control components, such as the main electrical and control panel, equipment local panels, power and control cabling, cable conduits and cable trays.

#### 4.6.6 Mist Eliminator

The bioreactor tank contains 10 compartments and one mist eliminator will be installed on top of each compartment. The mist eliminator is the only air exit of the compartment. The quoted price for the mist eliminator is estimated.

#### 4.6.7 Water Heater and Temperature Controller

Water heater and temperature control unit is needed to control the bioreactor liquid temperature to the range of 40°C. The overall BioGenerator reaction is exothermal and produces energy and heat. As the bioreactor liquid is continuously circulated, the system is considered a closed loop system. In the closed loop system, usually, the heat of the system is highly maintained, particularly, when the supplied air to the bioreactor has higher temperature than the bioreactor liquid temperature. Furthermore, the bioreactor tank is recommended to be constructed under the ground level in order to reduce the heat losses. However, in order to calculate the expected heat losses and how much energy is needed to maintain the bioreactor liquid temperature within the desirable range, real information of the climate profile of the intended site location is needed. Therefore, the quoted price of this item is estimated price and it is only budgetary price.

#### 4.6.8 Electrochemical Cell Stack Units

This is the second main component of the BioGenerator. Both electrochemical stack of the BioGenerator and PEM fuel cell are unavailable commercially. However, there are many price estimation studies for PEM fuel cell, and herein, one of these studies was used, taking into consideration the similarities and differences between PEM and the electrochemical stack of the BioGenerator. The used study was the most recent cost analysis of a PEM fuel cell [16]. The cost analysis of a stationary PEM fuel cell is summarized in Table 4. The cathode and the membrane costs were corrected to take into



account the specifics of the BioGenerator. Table 4 is based on low temperature PEM fuel cell with 10,000 manufacturing units per year.

**Table 4. Cost of all elements comprise the electrochemical stack unit.**

<b>Electrochemical Stack Unit Component Description</b>	<b>Total Cost for 1 MW power supply Capacity, USD</b>
Bipolar plates	7,300
Anode assembly: Membrane, catalyst ink, gas diffusion layer, and MEA frame.	34,200
Cathode	1200
End plates	800
Current collectors	100
Compression bands	1200
Stack housing	6400
Stack assembly	2100
Stack conditioning	2500

Total per stack	55,800
Total, all stacks	222,700
Total, \$/kW(net)	223

#### 4.6.9 Overall BioGenerator Cost Analysis

The individual prices of all components of the BioGenerator are summarized in Table 5, and the total estimated capital cost of one megawatt BioGenerator is also shown in the same table. The life time and the maintenance cost of each BioGenerator component are estimated to give an indication of the expected annual total maintenance cost.

**Table 5. Summary of the individual and total capital cost of all BioGenerator components.**

Item	Component Description	Capital cost, USD	Expected life time, year	Expected annual capital cost (\$/yr)	Expected maintenance cost per year, % of component's capital cost	Expected maintenance cost per year, USD
------	-----------------------	-------------------	--------------------------	--------------------------------------	---	---

1.	Civil and construction work; including excavation, compaction, backfilling, soil testing, RC construction of the bioreactor tank and plant room, water proofing, and internal acid resistant epoxy painting	2,070,000	40	51,750	1.0%	20,700
2.	Circulating pumping station	40,000	10	4,000	10%	4,000
3.	Air blower station	60,000	10	6,000	10%	6,000
4.	Pipes and fitting for the whole	160,000	15	10,667	5%	8,000

	plant					
5.	Mist eliminator unit	50,000	15	3,333	5%	2,500
6.	Water heating and temperature control unit	50,000	10	5,000	5%	2,500
7.	Electrical and control	250,000	15	16,667	2.5%	6,250
8.	Electrochemical stack unit	223,000	2	111,500	5%	11,150
9.	Miscellaneous	100,000	-		-	
	Total cost	3,003,000		208,917		61,100

With the assumption that the BioGenerator will produce full capacity electricity at 50% of the time (i.e., 4380 hours per year), the cost of electricity due to the BioGenerator is  $\$270,017 / (4380\text{h} \cdot 1000\text{kW}) = \$0.062 / \text{kWh}$ .

## 4.7 Discussion and Conclusion

This study presents the cost of the first industrial size of bio-electrochemical device for power generation at a scale of 1MW power generation. The cost calculation practically, includes all components of the BioGenerator.

In this chapter, the cost analysis is presented as a budgetary prices which primarily were based on valid price-lists, updated price-lists and some estimated prices based on North America local prices. It should be noted that the given prices are expected to differ significantly over different world-wide locations, and in some locations may they may be lower by 10-30%.

Unlike rechargeable batteries, the BioGenerator has a unique feature. It can operate at any time for unlimited period of time without the need of recharging, all it needs, is continuous supply of hydrogen and ferric ions solution. This unique feature put the BioGenerator in a very good position compared to all types of power storage rechargeable batteries which can only operate for few hours before their dire need to be recharged for longer period of time.

From table 5, the annualized capital cost of the BioGenerator is \$209,000/year, and the capital cost per kW is \$3,000/kW. The cost of electricity due to the BioGenerator is 6.2 cents per kWh.

The BioGenerator needs approximately 180 kW of electricity to run its electro-mechanical equipment needed to run the BioGenerator and produce one megawatt of electricity.

## 4.8 References

- [1] F. S. Barnes and J. G. Levine, *Large Energy Storage Handbook*, CRC press, Boca Raton, USA (2011).
- [2] Ontario Society of Professional Engineers, OSPE Energy Task Force, *Electrical energy storage options report*, March 2015.,  
<https://www.ospe.on.ca/public/documents/presentations/electrical-energy-storage-options.pdf>
- [3] Sherif SA, Barbir F, Veziroglu TN. Wind energy and the hydrogen economy—review of the technology. *Sol. Energy* 78, 647-660 (2005).
- [4] Ayers K. 245th ACS National Meeting, New Orleans, LA, USA, April 7-11 (2013).
- [5] Hamnett A. Kinetics of electrochemical reactions. In: *Handbook of Fuel Cells*, Eds.: Vielstich et al., Wiley, 2003, p. 34.
- [6] Qin C, Wang J, Yang D, Li B, Zhang C. Proton exchange membrane fuel cell reversal: a review. *Catalysts* 6, 1- 21 (2016).
- [7] D. Karamanev, Biofuel Cell, US Patent #2006251959 (2003).
- [8] Penev K, Karamanev D. Batch kinetics of ferrous iron oxidation by *Leptospirillum ferriphilum* at moderate to high total iron concentration. *Biochem. Eng. J.* 50, 54-62 (2010).

- [9] V. Pupkevich, Scale-up and study of the BioGenerator, PhD Thesis, University of Western Ontario (2014).
- [10] K Penev, D Karamanev, Kinetics of ferrous iron oxidation by *Leptospirillum ferriphilum* at moderate to high total iron concentrations, *Advanced Materials Research* 71, 255-258 (2009).
- [11] Pupkevich V, Glibin V, Karamanev D. The effect of activation on the electrochemical behaviour of graphite felt towards the  $\text{Fe}^{3+}/\text{Fe}^{2+}$  redox electrode reaction. *Electrochem. Comm.* 9, 1924–1930 (2007).
- [12] JM Gohil, DG Karamanev, Novel pore-filled polyelectrolyte composite membranes for cathodic microbial fuel cell application, *Journal of Power Sources* 243, 603-610 (2013).
- [13] R Balgobin, B Garcia, D Karamanev, V Glibin, Preparation and proton conductivity of composite  $\text{SiO}_2/\text{Poly}(2\text{-hydroxyethyl methacrylate})$  gel membranes, *Solid State Ionics* 181 (31), 1403-1407 (2010).
- [14] H Hojjati, K Penev, VR Pupkevich, DG Karamanev, Modeling, simulation, and optimization of hybrid  $\text{Fe(II)}/\text{Fe(III)}$  redox flow fuel cell system, *AIChE Journal* 59 (6), 1844-1854 (2013).
- [15] Metcalf and Eddy, *Wastewater Engineering Treatment and Reuse*, Fourth Edition, Chapter 5, page 429, McGraw Hill Education, 2003.

- [16] B. James, A. Spisak, W. Colella, Manufacturing cost analysis of stationary fuel cell systems, Strategic Analysis Inc., 2012.



## Chapter 5

### 5 Conclusions

- The BioGenerator is considered to be a viable alternative for energy storage particularly with the renewable energy supply (i.e. wind and solar). The power at off peak periods will be used to produce and store hydrogen, which will be used at the BioGenerator to generate electricity at low supply of wind or solar.
- Compared with rechargeable batteries that used for energy storage, The BioGenerator is more cost-effective solution. It can generate electricity, as far as hydrogen is supplied, for long periods without the need for recharging, dissimilar to rechargeable batteries which operate for few hours and need long time of recharging.
- The BioGenerator comprises mainly of bioreactor and electrochemical stack. In this study, a trickling bed bioreactor was used instead of the initially used airlift type. Some dynamics studies were conducted to investigate the effect of many different periods stoppage on the microbial culture efficiency. The study concluded no change in the microbial culture efficiency when stopping the substrate feed for up to 6 hours. However, when increasing the substrate feed stoppage to more than 16 hours, the microbial culture efficiency drops slightly and reaches up to 6% when stopping the substrate feed for 72 hours. However, the

microbial culture efficiency tends to recover quickly with time and usually returns to its original ferrous oxidation rate at continuous substrate feed supply. These important findings would emphasize the strong stability of the ferrous oxidation microbial culture and its quick recovery after long shortage of the substrate (ferrous ions and oxygen).

- Another study was conducted, aimed to model and upscale theoretical design of 1 MW BioGenerator. In this study the cost of the 1 MW BioGenerator was analyzed, the annualized capital cost of the BioGenerator is \$209,000/year, the capital cost per kW is \$3,000/kW, and the cost of electricity due to the BioGenerator is 6.2 cents per kWh. The theoretical efficiency of the BioGenerator is 82% based on generating power minus consumed power. That information is very important when considering power storage option.

## Chapter 6

### 6 Recommendations

- The BioGenerator needs to be further studied for its advancement and development. The researches should focus on; applying different types of bioreactor in order to increase the ferrous oxidation rate, increasing the oxygen transfer rate hence reducing the power consumed to operate the BioGenerator, extending the life time of the electrochemical stack by applying different bipolars and membranes materials and configurations.
- The BioGenerator is still in its emerging stage and needs more research and investigation till it can be commercialized. Oxygen transfer rate is a significant parameter of the BioGenerator operation, it consumes about 70% of the total power needed to operate the BioGenerator, and therefore, any increase in the oxygen transfer rate would contribute in major saving in the BioGenerator operation. Exploring different types and configurations of the bioreactor would lead to optimum bioreactor design that save in the operation cost. Trickling bed bioreactor is an important alternative for the Biogenerator, this type of bioreactors depends on circulating the bioreactor liquid and dissolving the oxygen from the air. It uses circulating pumps and doesn't need air blowers to transfer the oxygen, hence it is expected to have lower operational cost.

- It was observed that the ferrous oxidation rate is higher in the Trickling bed bioreactor compared to Airlift type. In the Trickling bed bioreactor the ferrous oxidation microbial culture is immobilized as attached on the supporting media and suspended in the liquid of the bioreactor. Further studies could confirm this observation and lead to increase the ferrous oxidation rate. Higher ferrous oxidation rate means smaller bioreactor size.
- The second main component of the Biogenerator is the electrochemical stack. This item is not commercialized yet and needs a lots of studies and development. Its bipolar plates need to be catalyzed with precious metals which are easily poisoned by carbon monoxide. The electrochemical stack suffers short life time which leads to dramatic increase in the BioGenerator cost. Extensive studies are needed to improve the life time and reduce the operation cost. The proton exchange membrane is also another main item of the electrochemical stack, it selectively passes the protons from the anode to the cathode and incorporates in producing the electricity. Selecting proper membrane is essential for better efficiency of the electrochemical stack.
- Many studies were conducted on the microbiology of the ferrous oxidation culture which led to *Leptospirillum ferriphilum* as the optimum bacteria for ferrous oxidation, these studies also led to the optimum temperature and pH range for the microbial growth. *Leptospirillum ferriphilum* is chemo-autotrophic bacteria oxidizes ferrous ions and uses carbon dioxide as the carbon source. Further studies can also be conducted on this type of bacteria to check the possibility of changing its behavior to mixotrophic and its use of glucose as carbon source

instead of carbon dioxide, and whether this change in behavior leads to change in the ferrous oxidation rate or not

## Curriculum Vitae

**Name:** Tariq Abou Jarboua

**Post-secondary Education and Degrees:** University of Western Ontario  
London, Ontario, Canada  
2012- 2013 M Eng. Chem. & Biochemical Eng.  
The University of Western Ontario, London, Ontario, Canada  
2015-2017 M.E. Sc. Chem. & Biochemical Eng.

**Related Work Experience:** Teaching Assistant  
University of Western Ontario  
2015-2016

Process Engineer, Project Manager  
R.V. Anderson, Alamr Consulting Group, Projects and Trading Co.2008-2014

### Publications:

Abou Jarboua T., Nikolov B., Karamanev D. (2017). Study of the dynamics of ferrous iron biooxidation by *Leptospirillum ferriphilum* in a trickling bed bioreactor used for energy storage (submitted to Biochemical Engineering Journal).

Abou Jarboua T., Karamanev D. (2017). Cost analysis of a 1 Megawatt bio-electrochemical technology, the BioGenerator (submitted to Journal of Applied Energy).